Strong Primary Contribution to Brown Carbon Light Absorption in Tibet and Urban Areas:

Insights based on in situ measurements

Wenhui Zhao[1,2], Weiwei Hu[1,3,4*], Zhaoce Liu[1,2], Tianle Pan[1,2], Tingting Feng[1,2], Jun Wang [1,2], Yiyu Cai[1,2], Lin Liang[5,6],Shan Huang[5,6*], Bin Yuan[5,6], Nan Ma[5,6], Min Shao[5,6], Guohua Zhang[1,3,4], Xinhui Bi[1,3,4], Xinming Wang[1,3,4],Pengfei Yu[5,6]

1. *State Key Laboratory of Advanced Environmental Technology, Guangzhou Institute of Geochemistry, Chinese Academy of Sciences, Guangzhou, 510640, China;*

2. *University of Chinese Academy of Sciences, Beijing 100049, China;*

3. *Guangdong–Hong Kong–Macao Greater Bay Area Environmental Pollution Research and Control Joint Laboratory, Guangzhou Institute of Geochemistry, Chinese Academy of Sciences, Guangzhou 510640, China;*

4. *Guangdong Key Laboratory of Environmental Resource Utilization and Protection, Guangzhou Institute of Geochemistry, Chinese Academy of Sciences, Guangzhou 510640, China;*

5. *College of Environment and Climate, Jinan University, Guangzhou 511443, China;*

6. *Guangdong–Hongkong–Macau Joint Laboratory of Collaborative Innovation for Environmental Quality, Guangzhou 511443, China*

*Correspondence to: Weiweihu@gig.ac.cn; shanhuang_eci@jnu.edu.cn

Abstract

To investigate optical properties, sources, and radiative effects of brown carbon (BrC), we conducted synchronous field campaigns in the Qinghai–Tibet Plateau (Yangbajing) and urban Guangzhou in July 2022, using multi-wavelength Aethalometer (AE33) and aerosol mass spectrometer (AMS) measurements. Total aerosol and BrC light absorption coefficients at 370 nm (Abs_{total}: 1.6 ± 1.6 M m^{-1}; BrC: 0.2 ± 0.3 M m^{-1}) in Tibet were an order of magnitude lower than Guangzhou, attributed to extremely low aerosol/organic aerosol (OA) mass concentrations. However, BrC fractions in Abs_{total} (15 % vs. 21 % at 370 nm) correlated with primary OA (POA) ratios, highlighting anthropogenic emission impacts even in this clean background. Diurnal variations (morning/evening peaks) of source–specific BrC absorption were regulated by local emissions (e.g., biomass burning, traffic emission) and regional secondary formation. Source apportionment revealed primary sources (biomass burning OA (BBOA), hydrocarbon-like OA (HOA)) dominated BrC absorption (> 75 %). The mass absorption cross–section (MAC) of HOA (2.08 m² g^{-1} in Tibet; 2.57 m² g^{-1} in Guangzhou) was comparable to that of BBOA (1.11–2.54 in Tibet; 1.91 m² g^{-1} in Guangzhou), indicating the high light absorption capacity of BrC from fossil fuel. Integrated "simple forcing efficiency" (370–660 nm) showed primary emissions contributed > 98 % of total radiative forcing at both sites. This study advances understanding of BrC dynamics and sources in diverse environments, underscores primary sources' critical role in BrC absorption, and emphasizes the need for source–specific OA optical parameterization.

Keywords:

Brown carbon; Source apportionment; Multiple linear regression; Optical properties; Radiative forcing

1. Introduction

Light absorbing components of atmospheric aerosols comprise black carbon (BC) and light absorbing organic aerosols, known as brown carbon (BrC). The BrC exhibits significant absorption in the near-ultraviolet (300–400 nm) and visible ranges (Andreae and Gelencsér, 2006; Kirchstetter and Thatcher, 2012; Laskin et al., 2015), but it remains largely overlooked in most climate models (Chung et al., 2012). Feng et al. (2013) found that accounting for the strong absorption of BrC in model could shift the global mean direct radiative forcing of OA at the top of the atmosphere from a cooling of −0.08 Wm^{-2} to a warming of +0.025 Wm^{-2}, emphasizing the significant role of BrC in global and regional direct radiative forcing of carbonaceous aerosols. Wang et al. (2025) revealed that dark BrC, emitted by wildfires and agricultural burning, strongly absorbs solar radiation, thereby generating a radiative effect of +0.02 to +0.68 Wm^{-2}, which contributed comparable warming as BC. Current global model simulation studies have demonstrated that the impact of BrC can contribute 12–50 % of the total positive radiative forcing from light-absorbing atmospheric aerosols and can be regionally different, which emphasizes the spatially dynamic variation of BrC and its important role in atmospheric warming (Li et al., 2025; Brown et al., 2018; Feng et al., 2013; Wang et al., 2018; Xu et al., 2024),.

In general, the source of atmospheric BrC can be categorized by direct emission (primary BrC) and secondary generation (secondary BrC) (Laskin et al., 2015). Over the past decade, primary BrC was found to be dominated by biomass burning, and the absorption capacity of BrC from fossil fuel is often neglected (Saleh, 2020). However, more and more recent studies have shown that fossil fuels (vehicle emissions and coal combustions) are also important contributors to the BrC, which have been previously underestimated (Du et al., 2014; Kasthuriarachchi et al., 2020a; Xie et al., 2017; Huang et al., 2022; Tang et al., 2020). Wang et al. (2022b) conducted a comprehensive review of the relationship between the source and light absorption characteristics of BrC based on the measurement results in China, positing that the emission and light absorption capacity of BrC from fossil fuel combustion might be comparable to or even exceed those induced by biomass burning. This finding raises the question of how much primary fossil and non-fossil sources contribute to ambient BrC. Regarding secondary BrC, its formation involves complex gaseous, particulate, and liquid-phase reactions from diverse precursors (Laskin et al., 2015). E.g., the nitro compounds formed through NO_3 oxidation or OH oxidation under high NO_x chemistry can lead to a significant enhancement in light absorption within the ultraviolet–visible (UV–Vis) range (Li et al., 2020; Jiang et al., 2019). Aqueous reactions of carbonyl groups with reduced nitrogenous organic compounds, such as organic amines and ammonium, are also found to be important BrC sources (Powelson et al., 2014; Tang et al., 2022).

The complex sources and multi–forming pathways of BrC make its global simulation a great challenge, e.g., mass absorption cross–section (MAC), which serves as a crucial optical parameter in simulating the BrC light absorption and further its radiative forcing, is still not clear due to the impact of multiple factors. E.g., various studies have demonstrated that the BrC light absorption properties are susceptible to the sources (Tang et al., 2020), photochemical aging (Yu et al., 2016; Wong et al., 2017; Lee et al., 2014; Zhao et al., 2015), humidity (Kasthuriarachchi et al., 2020b), acidity of aerosols (Mo et al., 2017; Phillips et al., 2017), and structure of chromophores (Laskin et al., 2014; Hems and Abbatt, 2018). In general, the MAC of secondary BrC was found to be generally lower than primary sources in ambient BrC (Qin et al., 2018; Zhang et al., 2022b). Smog chamber experiments also show that the MAC of aged coal combustion emission (0.14 ± 0.08 m^2 g^{-1}) was much lower than that of primary emissions (0.84 ± 0.54 m^2 g^{-1}) (Ni et al., 2021). If the impact of the atmospheric aging on MAC is not considered in the model, the simulated BrC light absorption may be overestimated by 45 % to 128 % (Li et al., 2025). In addition, Li et al. (2025) pointed out that the uncertainty in the effective MAC of primary BrN (i.e., absorptive nitrogenous component of BrC) from anthropogenic and biomass burning has the greatest impact (reaching ±76 % uncertainty) on the simulated BrN light absorption, highlighting the key role of source–specific MAC in the global simulation of BrC light absorption. Further clarification of the MAC of BrC from different sources in the ambient air is imperative, which can greatly help to improve the understanding of BrC light absorption and the model simulation. However, the total contribution to ambient BrC from SOA and POA and their source–specific MAC values is still ambiguous due to varied regions and circumstances, which warrants further study.

Due to the complexity and diversity of BrC, in conjunction with black carbon (BC), which share similar combustion sources and complex mixture states (Bond and Bergstrom, 2006; Cappa et al., 2012; Cappa et al., 2019), it remains challenging to measure the source–specific BrC light absorption in the

ambient air directly. The field measurement on ambient BrC begins with filter–based offline methods using solvent (water or organic solvent) extraction (Bond and Bergstrom, 2006). One of the limits of the offline technique is the low time resolution (usually 12–24 hours), which cannot reflect the dynamic variation of BrC during a day. As measurement techniques have developed, online methods for aerosol light absorption at different wavelengths have become available (Lack et al., 2014). The most widely used instruments include multi–wavelength Aethalometers (AE31/AE33) (Drinovec et al., 2015) and three–wavelength multi-pass Photo Acoustic Spectroscopy (PAS) (Lack et al., 2012). The online measurements can provide dynamic variations in BrC light absorption at high time resolution (1 minute). Together with source apportionment techniques, source contribution to BrC at high time resolution can be obtained, which can greatly aid in understanding the dynamic characteristics of ambient BrC and its sources.

Currently, most of the field studies focusing on ambient BrC and its sources are conducted in urban areas (Qin et al., 2018; Sun et al., 2021; Wang et al., 2019b; Zhong et al., 2023), while the BrC contribution in regional background areas is still limited. The Qinghai–Tibet Plateau (QTP) region, spanning approximately 2.5 million square kilometers, is acknowledged as the world's highest plateau (Yao et al., 2012). The atmosphere in QTP can substantially influence the climate in the world. E.g., the light–absorbing carbonaceous aerosols have been identified as one of the main factors causing the accelerated glacier retreat across the QTP (Usha et al., 2022; Kang et al., 2019; Chelluboyina et al., 2024). Compared to the southern and northern regions of the QTP, anthropogenic BC is the dominant driver of glaciers melt in the central QTP, whose radiative forcing can be up to 17 times greater than that in the southern QTP (Li et al., 2017; Ming et al., 2013). Moreover, a portion of the glaciers in central QTP are situated in the headwaters of the Yangtze River, thus, the melting directly impacts the livelihoods of millions of people downstream. The melt sensitivity of these glaciers to light-absorbing impurities (such as OA, BC and mineral dust) is not only higher than that of their southern counterparts but also carries greater regional ecological and social significance (Li et al., 2017). Although BrC is an important light-absorbing OA, limited studies on its variation and sources have been conducted in the central QTP, and most have focused on the edge of the southern region(Wang et al., 2019a; Zhang et al., 2021; Tian et al., 2023). We found that cross-border transport of biomass burning from South Asia was responsible for a significantly higher BrC light absorption contribution in the southern QTP than in the central and northeastern regions. However, OA in the central QTP not only originated from long-range transport (Xu et al., 2018), but anthropogenic activities also have a significant impact on the OA sources, such as local biomass burning and fossil fuels (Xiang et al., 2024). Field measurements in the central QTP can improve our understanding of how human activities in remote regions impact light-absorbing aerosols and, consequently, glacial melting and radiative forcing. In central QTP, only one source apportionment of the light absorption of offline water–soluble BrC was reported (Zhu et al., 2024), which showed a large contribution of biomass burning (29 %), fossil fuel combustion (17 %) and secondary contribution (54 %) to the total BrC light absorption. Further clarification is still needed. In addition, although the online BrC data have been reported in the Tibet region, the dynamic variation of BrC and its source contribution is seldom shown (Zhang et al., 2021; Wang et al., 2024; Chen et al., 2024; Wang et al., 2019a; Tian et al., 2023; Zhu et al., 2021; Zhu et al., 2017). The investigation of the dynamic variation of BrC, e.g., diurnal

variation, can greatly promote the understanding of BrC fate in the ambient air, which shall be further studied.

In this study, the real–time measurement of OA and light absorption of aerosols was carried out in the background site of central QTP. For comparison, a concurrent campaign was also carried out during the same period in a typical megacity of China, Guangzhou. The comparison results from distinct two environments at the same time can help better understand the light absorption capacity of BrC in QTP. In both campaigns, an online multi–wavelength Aethalometer (AE33) was applied to characterize the dynamic variation of BrC. The positive matrix factorization (PMF) method together with aerosol mass spectrometer (AMS) data was used to apportion the sources of OA. The multiple linear regression (MLR) was used to explore the possible dynamic source contribution to BrC in two representative regions. Finally, source–specific BrC to light absorption and the radiative forcing in remote and urban areas was shown.

2. Methodology

2.1. Sampling sites

The field campaigns were simultaneously conducted from July 3 to August 3, 2022 in Tibet, and from July 16 to August 5, 2022 in urban Guangzhou, as depicted in Fig. 1. The Yangbajing site (YBJ site; 30.2°N, 90.45°E; 4,300 m above sea level [a.s.l.]) serves as a background location situated in the central QTP, approximately 90 km northwest of Lhasa City. With a permanent population of around 6,000, YBJ was supposed to be influenced by mixed plumes of regional transportation, while local anthropogenic emissions (e.g., light traffic flow and/or fuel combustion for domestic heating or cooking activities) were also found (Liu et al., 2021; Xiang et al., 2024). The urban site (GIG site; 23.1 °N, 113.4°E; 53 m a.s.l.) is set on the campus of the Guangzhou Institute of Geochemistry, Chinese Academy of Sciences (CAS), located in the downtown area of Guangzhou (permanent population: ~20 million). The GIG site is surrounded by transportation, commercial, and residential areas (Chen et al., 2021). During the whole campaigns, lower temperature and Relative Humidity (RH) were observed in the YBJ site (13.4 ± 4.6 ℃, 52.1 ± 21.9 %) than those in the GIG site (29.5 ± 2.8 ℃, 82.9 ± 12.7 %), which is expected due to the high altitude of Yangbajing (4,300 m) compared to Guangzhou (53 m). Southeast and north winds were dominant throughout the observation period at the YBJ site with an average wind speed of 2.3 ± 1.6 m s^{-1}, while the GIG site was dominated by south and southwest winds at a speed of 2.2 ± 0.9 m s^{-1}, as shown in Fig. 1. The date and time used in this study are reported using Beijing Time (BJT: UTC +8h).
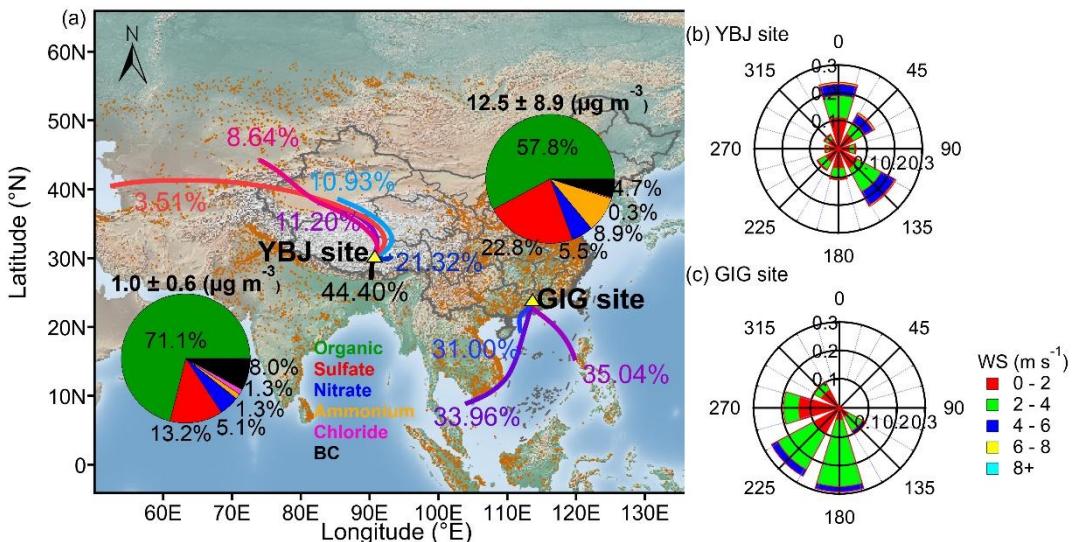
Figure 1. (a) Map of the locations of Yangbajing (YBJ) and Guangzhou (GIG) sites (yellow triangles). Solid colored lines represent the average back trajectory clusters during the whole campaign and the corresponding contributions plotted using the MeteoInfo version 2.2.6 developed by Wang (2019) (download from *http://www.meteothink.org*, last access time: 23 June 2025). The orange dots on the map indicate the location of the fire spot (download from *Active Fire Data Earthdata (nasa.gov)*, last access time: 14 December 2023). The pie charts represent the chemical compositions of submicron particulate matter (PM$_1$) along with their contributions at both sites during this campaign. The rose plots colored by wind speed (WS) at (b) the YBJ site and (c) the GIG site are also shown.

2.2. Light absorption coefficient measurement

The aerosol light absorption coefficients at both sites were measured by multi–wavelength Aethalometer (Model AE33, Magee Scientific Corp., Berkeley, CA, USA) at seven wavelengths (370, 470, 520, 590, 660, 880, 950 nm) with a high time resolution of 1 minute (Drinovec et al., 2015). Ambient aerosols were introduced into AE33 through a PM$_{2.5}$ cyclone at a flow rate of 5 L min^{-1}. The AE33 collected aerosols via continuous pumping to a specific location on the filter belt. It then measured the transmitted light that passed through this sample–containing spot and a corresponding blank filter film spot. The instantaneous light–absorbing aerosols were determined by analyzing the variation in the attenuation rate of the transmitted light across the particulate–loaded filter membrane. To accurately reflect the real optical absorption coefficients of airborne aerosols, a real–time compensation parameter (k value) and a fixed filter multiple scattering parameter (C$_{ref}$ = 1.57 for tetrafluoroethylene (TFE)–coated glass filter) are required to correct the optical attenuation coefficient measured on the filter membrane. For the k value, the "dual–point" measurement technique of AE33 avoids the "aerosol loading" effect during single filter tape membrane sampling, enabling real–time calculation corrections for load compensation parameters (Drinovec et al., 2015). Multiple studies have shown that the C value (2.8–7.8) varies with different wavelengths and observation locations (Qin et al., 2018; Collaud Coen et al., 2010; Tian et al., 2023; Zhang et al., 2021). In this study, the C$_{final}$ values of 3.34 (2.23* C$_{ref}$) for the YBJ site and 3.6 (2.3*1.57) for the GIG site were applied based on the previous studies in Tibet (Zhang et al., 2021) and Guangzhou (Cai et al., 2024), also using the AE33 instrument.

2.3. OA measurement and source apportionment

The main chemical compositions of submicron aerosols including OA, nitrate, sulfate, ammonium,

and chloride were measured using a soot particle time–of–flight aerosol mass spectrometer (SP–AMS; Aerodyne Research Inc., Billerica, MA, USA) (Onasch et al., 2012) at YBJ site and a time–of–flight aerosol chemical speciation monitor (ToF–ACSM; Aerodyne Research Inc., Billerica, MA, USA) (Fröhlich et al., 2013) at GIG site. During this campaign, both the SP–AMS and ToF–ACSM shared the same sampling inlet with co–located AE33. The setup diagram can be found in Fig. S1. The time resolution of SP–AMS and ToF–ACSM was 1 min and 40 s, respectively. For SP-AMS, dual vaporization mode and tungsten-only V mode were alternatively applied every 4 minutes. In this study, tungsten-only mode, which resembled the traditional HR-ToF-AMS, was applied. The ionization efficiency (IE) calibration was done using monodispersed NH_4NO_3 aerosols before and after campaigns. The relative ionization efficiency (RIE) of sulfate and ammonium is 1.26 and 4.24 for SP–AMS and 1.22 and 3.39 for ACSM, while a default RIE of 1.4 was used for OA. A constant collection efficiency (CE) of 0.5 was used for YBJ measurement due to the quite low mass fraction of ammonium nitrate (< 40 %), while the composition-dependent collection efficiency (average CDCE = 0.52) (Middlebrook et al., 2012) was applied in GIG measurement. The SP–AMS data were processed using SQUIRREL (v1.65) and PIKA (v1.25A), embedded in Igor Pro (v6.37; WaveMetrics, Inc., Lake Oswego, OR, USA), while ToF–ACSM data were processed using Tofware 3.2.4 (Tofwerk AG, Thun, Switzerland).

The positive matrix factorization (PMF) (Ulbrich et al., 2009; Zhang et al., 2011) was applied to the OA spectral matrix to resolve the sources of OA at both sites. More detailed information can be found in Text S1 and Table S2. The final OA source apportionment at the YBJ site and GIG site are shown in Fig. S4. At the YBJ site, five OA factors were finally resolved using free PMF with PMF3.05 (Ulbrich et al., 2009), including hydrocarbon–like OA (HOA, 11 %) mainly from traffic emissions, biomass burning OA (BBOA, 9 %), biofuel–OA (13 %), less–oxidized oxygenated OA (LO–OOA, 42 %), and more–oxidized oxygenated OA (MO–OOA, 25 %). At the GIG site, OA was resolved based on Multilinear Engine 2 (ME–2; SoFi 6.8) (Canonaco et al., 2013), and the standard BBOA mass spectra (Hu et al., 2016; Hu et al., 2013) were introduced as an external constraint to fully constrain (a value = 0) BBOA factor at the GIG site. Finally, five factors were chosen with MO–OOA (49 %) and LO–OOA (22 %) dominating the total OA, followed by cooking–related OA (COA, 13 %), BBOA (8 %), and HOA (8 %).

2.4.   Calculation of BC and BrC light absorption coefficients

The Absorption Ångström exponent (AAE) method was widely used to distinguish BC and BrC light absorption coefficients measured by Aethalometer (Lack and Langridge, 2013). Previous studies demonstrated that the aerosol light absorption at 880 nm was entirely dominated by BC (Kirchstetter et al., 2004). The absorption coefficients of BrC at shorter wavelengths (370, 470, 520, 590, and 660 nm) can be calculated by combining the AAE (Lack and Langridge, 2013) with BC light absorption at 880 nm, using the following Equations:

$$\mathrm{Abs}_{BC}(\lambda) = \mathrm{Abs}(880) \times \left(\frac{880}{\lambda}\right)^{\mathrm{AAE}_{BC}} \quad (1)$$

$$\mathrm{Abs}_{BrC}(\lambda) = \mathrm{Abs}(\lambda) - \mathrm{Abs}_{BC}(\lambda) \quad (2)$$

Here, $\mathrm{Abs}_{BC}(\lambda)$ and $\mathrm{Abs}_{BrC}(\lambda)$ (M m^{-1}) represent light absorption coefficients of BC and BrC at wavelength λ (nm), respectively. $\mathrm{Abs}(\lambda)$ represents the total aerosol light–absorbing coefficients at the

wavelength λ, which can be calculated by the mass concentration of BC (μg m^{-3}) multiplied by mass absorption cross–section (MAC; m^2 g^{-1}) at wavelength λ, denoted as $\text{Abs}(\lambda) = \text{BC}(\lambda) \times \text{MAC}(\lambda)$. In this study, default MAC values for BC (18.47, 14.54, 13.14, 11.58, 10.35, and 7.77 m^2 g^{-1} for 370, 470, 520, 590, 660, and 880 nm, respectively) were used (Drinovec et al., 2015). AAE$_{BC}$ denotes the wavelength dependence of pure BC particles, which was usually assumed as 1 to calculate the light absorption coefficient of BC (Tian et al., 2023; Zhang et al., 2022b). However, due to the multiple effects (e.g., lensing effect) caused by the mixing of non–BC/coating materials and BC during atmospheric evolution, the light absorption of BC can be enhanced (Jacobson, 2001; Liu et al., 2017; Peng et al., 2016). Moreover, AAE$_{BC}$ was also found to be varied as a function of absolute wavelength values (Luo et al., 2022), which was suggested as 0.8–1.4 for BC particles (Lack and Langridge, 2013; Kasthuriarachchi et al., 2020a; Zhai et al., 2022; Corr et al., 2012). We summarized the AAE$_{BC}$ values from the literatures in Table S3, and found all the actually used values are between 1 – 1.18. E.g., within one campaign (Kasthuriarachchi et al., 2020), 93% of directly measured AAE from ambient core BC in Singapore was found to be less than 1.1. An AAE$_{BC}$ of 1.4 represents a typical high value, considering the mixing of non-absorbing material with BC in the extreme case (Lack and Langridge, 2013). For our study, we found ~82% of data was negative value when the AAE$_{BC}$ of 1.4 was applied, which is unrealistic to apply here. Thus, to investigate the uncertainty of BrC estimated here, AAE$_{BC}$ of 0.8 to 1.2 was applied, which results in 2–13 % and 4–14 % of BrC contribution to total light absorption from 370 to 660 nm for the YBJ site and GIG site, respectively.

2.5. Sources contribution to BrC light absorption based on multiple linear regression (MLR)

To further understand the sources of BrC light absorption, a multiple linear regression (MLR) was used to apportion the BrC light absorption to different components resolved by the source apportionment of OA (Kasthuriarachchi et al., 2020a; Qin et al., 2018; Tian et al., 2023; Zhang et al., 2021), using the following Equations:

$$\text{Abs}_{\text{BrC}}(\lambda) = \sum(a \times Factor) + \text{intercept} \qquad (3)$$

Here, $\text{Abs}_{\text{BrC}}(\lambda)$ (M m^{-1}) represents the BrC light absorption coefficient at a wavelength of λ (370, 470, 520, 590 and 660 nm); a represent the regression coefficients of different OA components, which can be regarded as MAC (m^2 g^{-1}) values (Kasthuriarachchi et al., 2020a); $Factor$ (μg m^{-3}) represents the mass concentration of OA from different sources (see Sect. 2.3).

2.5.1. Uncertainty analyses for the MLR method

Multicollinearity is an important factor leading to inaccurate estimation of regression coefficients in the MLR model. To estimate the uncertainty of the MLR method, we tested different scenarios with varied PMF factor combinations based on their correlation. To compare with other published results and simplify the calculation process, the MLR uncertainty at 370 nm was estimated. In general, four cases were chosen for the YBJ campaign, and three cases were chosen for the GIG campaign by combining or excluding collinear factors. The detailed information can be found in Text S2 and Table S5. All the cases yield similar low coefficients for the SOA factor and high coefficient values for the POA factors, suggesting the validity of MLR analysis shown here.

With each solution, the uncertainty of the regression coefficient (i.e., MAC) for the individual OA components input into the MLR model was evaluated using Monte Carlo simulations. For the Monte Carlo calculation input, the uncertainty of the PMF factor mass concentration needs to be evaluated. A bootstrap analysis (100 iterations; (Ulbrich et al., 2009) was applied, which shows a 9–36 % uncertainty for the PMF factors at the YBJ site and 3–9 % at the GIG site, as shown in Table S6. The uncertainty for the coefficient of BrC at 370 nm was estimated to be 43 % for the YBJ site and 36 % for the GIG site based on the lower (0.8) and upper limit of (1.2) previously reported AAE_{BC} range. The total uncertainties of each coefficient for each PMF factor were then calculated by Monte Carlo with 10,000 simulations.

Considering that biomass burning is widely reported as an important source of BrC light absorption and regarded as a warming agent affecting global climate (Wang et al., 2025), we consider all biomass burning related contributing sources when run the MLR model in the case of eliminating the collinearity problem in this study. As previously reported in the literature (Kasthuriarachchi et al., 2020a; Qin et al., 2018), the MAC of COA is nearly zero, thus, the light absorption by COA at GIG site was not considered in this study. We finally combined the BBOA factor and Biofuel–OA factor as BBOA (case 3) for the YBJ site and included BBOA, HOA as input (case 3) for the GIG site (Table 1). The SOA (LO-OOA and MO-OOA) at GIG site were not inputted here due to the collinearity with BBOA, the light absorption contribution and MAC values (case 3) at GIG site will be lower limits for SOA. For its upper limits, Case 2 in the supporting information (Text S2; Table S5) was also shown (Fig. S9). At the YBJ site, the MAC uncertainty of BBOA (26.4 %), HOA (20.8 %), LO–OOA (56.3 %), and MO-OOA (57.9%) was found, as shown in Table S7. For the GIG site, the MAC uncertainty of HOA (5.8 %), BBOA (6.8 %), and intercept (21.6 %) was estimated. With the final solution, the total light absorption calculated from the predicted regression coefficients (i.e., MAC) showed strong agreement with the measured values, as indicated by the slopes (YBJ: 0.9; GIG: 0.9) and Pearson correlation coefficients (YBJ: R = 0.8; GIG: R = 0.7). These results suggest the robustness of the regression analyses. However, a notable intercept (0.37 M m^{-1}, representing 13 % of the total light absorption) was observed in the MLR model at the GIG site. This intercept indicates a portion of BrC light absorption that could not be explained by the OA factors, potentially due to uncertainties associated with the MLR method. The detailed discussion of MAC and BrC light absorption contributions is shown in Sect.3.2.

Table 1. Regression coefficients (MAC) of the final case of multiple linear regression (MLR) at 370, 470, 520, 590, and 660 nm at the YBJ site and GIG site. Note that the SD represents the Standard deviation purely calculated from the MLR model.

YBJ site					
	Wavelength (nm)				
MAC (Average ± SD)	370nm	470nm	520nm	590nm	660nm
biofuel–OA	1.11 ± 0.11	0.42 ± 0.05	0.11 ± 0.03	0.11 ± 0.02	0 ± 0.03
HOA	2.08 ± 0.3	1.11 ± 0.14	0.18 ± 0.10	0.16 ± 0.06	0 ± 0.07
LO–OOA	0.15 ± 0.08	0.14 ± 0.03	0.07 ± 0.02	0.04 ± 0.02	0.01 ± 0.02
MO–OOA	0.18 ± 0.18	0.19 ± 0.08	0 ± 0.06	0.02 ± 0.04	0 ± 0.04
Intercept	0 ± 0.02	0.02 ± 0.01	0.04 ± 0.01	0.02 ± 0	0.03 ± 0
GIG site					
	Wavelength (nm)				
MAC (Average ± SD)	370nm	470nm	520nm	590nm	660nm
BBOA	1.91 ± 0.21	0.90 ± 0.10	0.35 ± 0.06	0.40 ± 0.04	0.20 ± 0.02
HOA	2.57 ± 0.28	1.40 ± 0.13	0.72 ± 0.07	0.38 ± 0.06	0.13 ± 0.03

	Intercept	0.37 ± 0.17	0.18 ± 0.08	0.42 ± 0.04	0.17 ± 0.03	0.11 ± 0.02

2.6. Calculation of radiative forcing

The estimation of the direct radiative forcing caused by BrC was conducted using a model known as the "simple forcing efficiency (SFE)", which can provide a radiative forcing (W g^{-1}) based on a given mass of aerosols. Although the resulting value of SFE is lower than that projected by climate models, it still serves as a valuable tool for gauging the sensitivity of various input parameters (Bond et al., 2006; Chylek and Wong, 1995). In this study, we used a modified version of the wavelength-dependent SFE without considering mass scattering and expressed it as follows (Tian et al., 2023; Zhang et al., 2020a; Zhang et al., 2022b):

$$SFE(\lambda) = \frac{S(\lambda)}{4} \times \tau_{atm}^2 \times (1 - F_c) \times 4\alpha_s \times MAC(\lambda) \quad (4)$$

Here, $S(\lambda)$ (W g^{-1} nm^{-1}) is the wavelength–dependent solar irradiance based on the ASTM G173–03 Reference Spectra (https://www.nrel.gov/grid/solarresource/spectra–am1.5.html); τ_{atm} represents atmospheric transmission (0.79); F_c is the cloud fraction (0.6); α_s is the surface albedo (global average 0.19) (Chen and Bond, 2010). $MAC(\lambda)$ (m^2 g^{-1}) is the mass absorption cross–section of different OA components at wavelength λ at a 1 nm resolution. The $MAC(\lambda)$ can be calculated according to the power–law fitting results between the MAC from each OA component at different wavelengths (370 to 660 nm) in this study. Note that the SFE represents a straightforward calculation designed to ascertain the relative significance of diverse optical properties of radiative forcing. However, to accurately determine forcing efficiency, a comprehensive radiative transfer model is still necessary (Efremenko and Kokhanovsky, 2021).

3. Results and discussion

3.1. Overview of Aerosol light absorption

The summarized total aerosol light absorption coefficients (Abs$_{total}$) as a function of wavelength at two sites are shown in Fig. 2 and Table S8. The more detailed temporal evolutions of Abs$_{total}$ at two sites are displayed in Fig. S7, In general, the average Abs$_{total}$ ranged from 0.6 to 1.6 M m^{-1} (370 to 950 nm) at the YBJ site, while the 7–8 times higher Abs$_{total}$ (4.2–13.2 M m^{-1}) was observed at the GIG site (Fig. 2a and Table S8). This discrepancy was primarily attributed to the much higher aerosol mass concentration in urban Guangzhou (PM$_1$: 12.5 ± 8.8 μg m^{-3}) compared to the background Tibetan region (PM$_1$: 1.0 ± 0.6 μg m^{-3}) (Figs. 2a and 2b). The campaign-averaged BrC light absorption coefficients (Abs$_{BrC}$) and its contribution to total aerosol light absorption increased with decreasing wavelength at both sites (AAE of BrC is 2.6 for YBJ and 3.2 for GIG; Figs. 2c, 3b, and 3d), indicating strong BrC light absorption at shorter wavelengths. At 370 nm, where BrC contributes the most to the total light absorption, Abs$_{BrC}$ in Tibet (0.2 ± 0.3 M m^{-1}) was found to be a factor of 13 lower than that in Guangzhou (2.9 ± 2 M m^{-1}). This finding is consistent with the much lower OA mass concentrations (by a factor of ~10) at the YBJ site (OA: 0.7 ± 0.4 μg m^{-3} vs 6.9 ± 5.8 μg m^{-3} at GIG; Figs. 2b and 2c).. A positive correlation between BrC light absorption and OA mass concentration was also observed across different field studies (Fig.2d; Table S4). This relationship aligns with the findings of Wang et al. (2022a), who reported that

320 BrC light absorption at 365 nm positively correlates with OA mass concentration across various sources.

321 To facilitate a visual comparison with previous studies, the literature–reported BrC light absorption
322 results at 365 or 370 nm are summarized in Fig. 3e and Table S4. This wavelength was chosen due to its
323 higher BrC abundance across different wavelengths, which leads to less uncertainty. At the YBJ site, the
324 campaign-averaged Abs_{BrC} at 370 nm (0.2 M m^{-1}; 0.03–0.6 M m^{-1} for 5–95 % range; Table S4) was
325 lower than the values reported across the Qinghai–Tibet Plateau (QTP) (0.6–14.9 M m^{-1}), e.g., the BrC
326 light absorption at YBJ site (central QTP) was much lower than those observed at the edges of the QTP,
327 such as Ngari (5.9–10.7 M m^{-1}), Qomolangma Station (QOMS, 4.4 M m^{-1}), and Gaomeigu (12.3 M m^{-1}
328 ^{1}), where elevated values are primarily influenced by the cross–border transport of biomass burning
329 plumes during pre–monsoon or post–monsoon period (Zhang et al., 2021; Tian et al., 2023; Zhu et al.,
330 2017). The low BrC light absorption at YBJ can be attributed to the extremely low mass loading of OA
331 (0.7 ± 0.5 μg m^{-3}), which is influenced by wet deposition from precipitation and specific atmospheric
332 circulation patterns during July, a monsoon period (Xu et al., 2018; Zhao et al., 2013). In addition, the
333 absolute BrC light absorption coefficient at YBJ was comparable to levels measured in certain remote
334 regions, such as the Arctic (0.04–0.2 M m^{-1} at 365 nm) (Barrett and Sheesley, 2017; Yue et al., 2022; Yue
335 et al., 2019), highlighting the relatively clean atmospheric conditions at YBJ as a background site in Tibet.
336 In general, BrC light absorption in urban areas tends to be higher or comparable to that in QTP regions
337 due to typically higher OA mass concentrations (Fig. 2d).

338 Although a relatively large discrepancy in the absolute light absorption coefficient of BrC was
339 observed between the YBJ and GIG sites, the contribution of BrC to total aerosols (Fraction$_{BrC}$) was
340 comparable at both sites (15 % vs. 21 %), highlighting the significant role of BrC in light absorption at
341 both locations. We summarized Fraction$_{BrC}$ across different studies and regions, as shown in Fig. 3e and
342 Table S4, which reveals that Fraction$_{BrC}$ values generally fall within a range of 8–58 %. Notably, the
343 Fraction$_{BrC}$ in the Qinghai–Tibet Plateau (QTP) is comparable to that in urban areas. Furthermore, a clear
344 trend shows that Fraction$_{BrC}$ at the edges of the northeastern (such as Qinghaihu Lake) and south QTP
345 (such as Ngari) tends to be higher than in the central QTP (such as Beiluhe, Namco, and YBJ site), and
346 the Fraction$_{BrC}$ in Northern China is generally higher than in Southern China. To better understand the
347 factors driving the Fraction$_{BrC}$, we investigated the relationship between the contribution of primary
348 organic aerosol (POA) and secondary OA (SOA) to total OA and the Fraction$_{BrC}$. As illustrated in the
349 inset plot of Fig. 3e, a positive correlation was observed, suggesting that the enhanced POA contribution
350 will increase the BrC light absorption contribution in carbonaceous aerosol. For sites at the edges of the
351 QTP and in northern Chinese cities, where the Fraction$_{BrC}$ is higher, OA is significantly influenced by the
352 combustion of solid fuels, including coal and biomass, particularly during winter. This finding signifies
353 the importance of POA in contributing to ambient BrC light absorption.
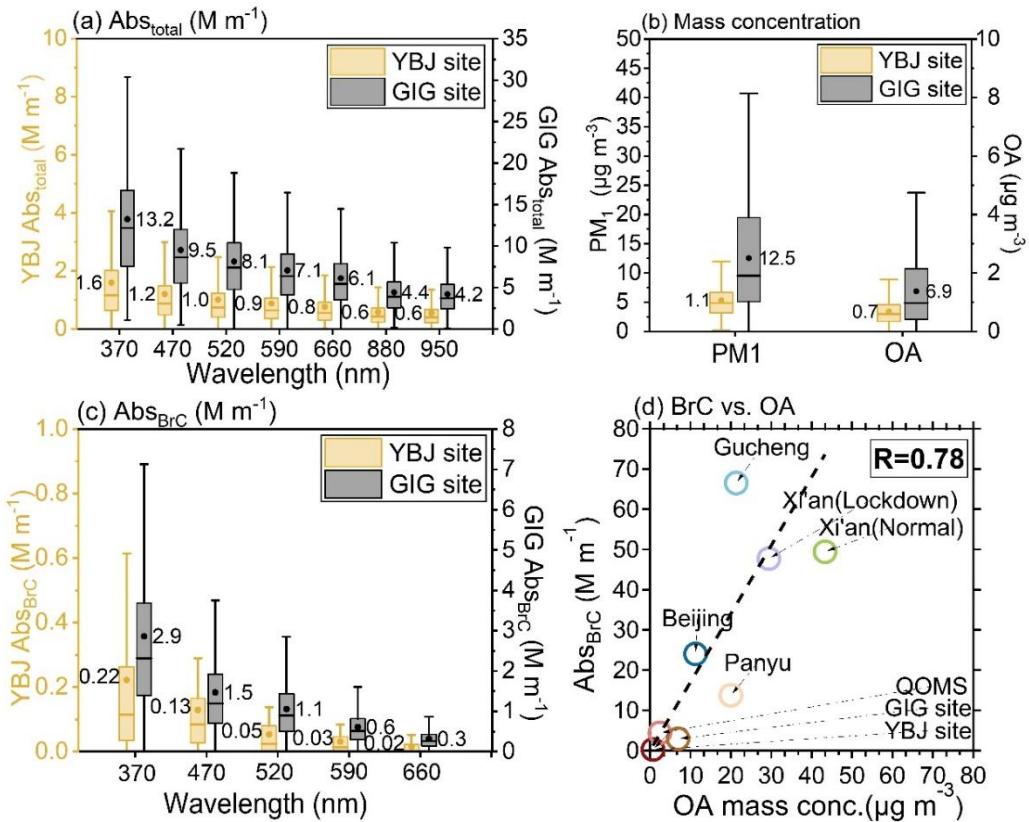
Figure 2. Box plot of the light absorption coefficient of total aerosols (Abs_{total}) (a) and BrC (Abs_{BrC}) (c)
from 370nm to 950nm at YBJ (left Y axis) and GIG (right Y axis) sites. The Abs_{BrC} was separated from
the Abs_{total} based on Eq. (1) and (2) using $AAE_{BC}=1$, (b) Box plot of PM_1 and OA mass concentrations
at the YBJ site and GIG site. The whiskers indicate the 90th and 10th percentiles, the upper and lower
boundaries of boxes indicate the 75th and 25th percentiles, the lines in the boxes indicate the median
values, and the markers for the mean values. (d) Scatter plot of the BrC absorption coefficient as a
function of OA concentration (data from the literature (Table S3)).
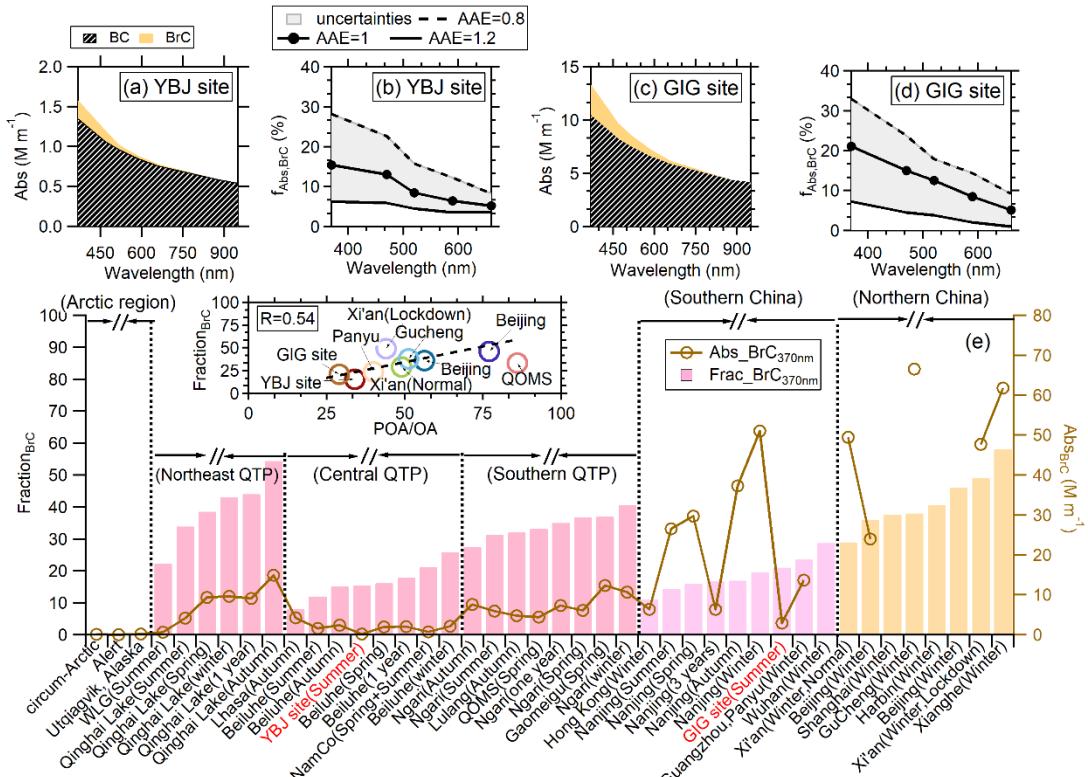
Figure 3. The absolute light absorption coefficients of BC (Abs_{BC}) and BrC (Abs_{BrC}) at wavelengths from 370 to 880 nm at the (a) YBJ site and (c) GIG site, respectively. The BrC was calculated based on the AAE of BC (AAE_{BC})=1. The contribution of BrC light absorption at wavelengths from 370 to 660 nm at the (b) YBJ site and (d) GIG site, respectively. The grey–filled area represents variations in the BrC light absorption fraction caused by the AAE_{BC} from 0.8 (dashed line) to 1.2 (solid line). The circle makers are the average value estimated based on AAE_{BC}=1. (e) The summary of BrC light absorption coefficients (the brown circles) and their contributions to total light absorption coefficients at 370 nm from the literature results. The results were categorized according to the locations of their observation sites (Arctic region, Qinghai–Tibet Plateau (QTP region), Southern China, and Northern China). The inset plot represents the relationship between the BrC light absorption fraction and the contribution of primary OA to total OA. The detailed information is provided in Table S4.

To further elucidate the dynamic evolution of BrC light absorption, the diurnal variations of $Abs_{BC,370}$ and $Abs_{BrC,370}$ were displayed in Fig. 4 (Abs_{total} at different wavelengths was shown in Fig. S8). $Abs_{BC,370}$ and $Abs_{BrC,370}$ at both sites peaked simultaneously, indicating combustion source for BC are also important contributor to the BrC in both studies. At the YBJ site, the peaks at 08:00 and 22:00 align with the NO_x ($NO + NO_2$) and CO, which were due to the local or regional anthropogenic emissions (such as vehicle emissions and other combustion activities) in Tibet. In other periods, a background $Abs_{BrC,370}$ value of 0.19 M m^{-1} was found at YBJ site. The diurnal patterns of $Abs_{BC,370}$ and $Abs_{BrC,370}$ at the GIG site, which showed an enhancement at 10:00 and a stronger peak at 21:00, were slightly different from those at the YBJ site. This difference suggests distinct source emissions or secondary formation patterns between the two locations (Fig. 4b and Fig. S8b). Higher increase of NO_2/NO and CO at night in Guangzhou was also found, implying the potentially important contribution of vehicles and other combustion sources, e.g., biomass burning, at this urban site.
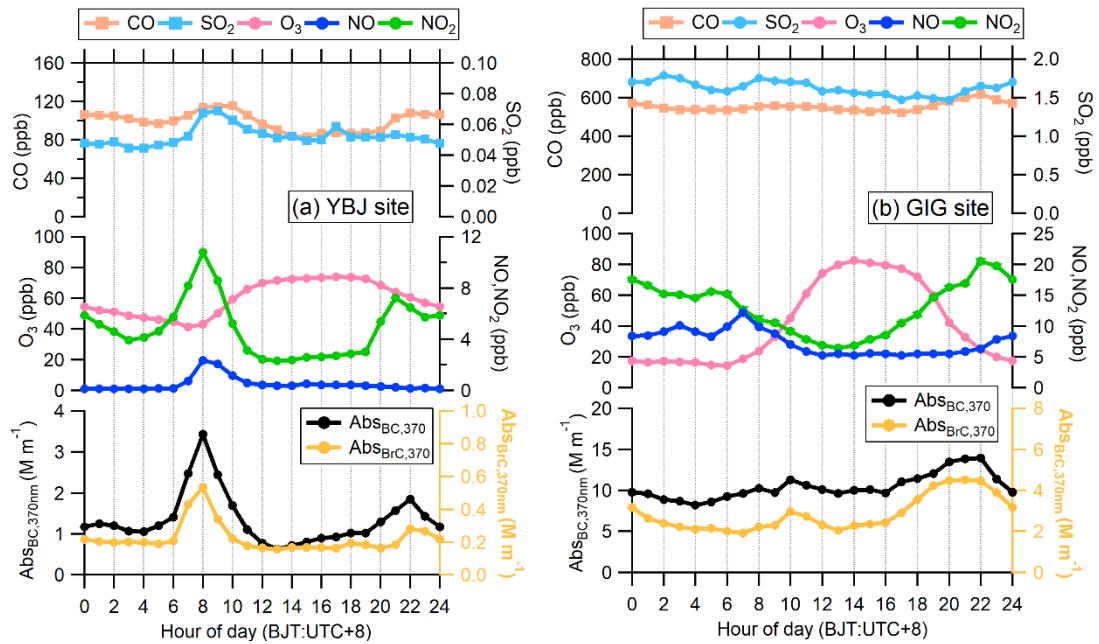
Figure 4. Diurnal variations of gas pollutants and BC/BrC light absorptions at 370 nm at (a) YBJ site and (b) GIG site.

3.2. Optical properties of source–specific BrC

To further identify the source of absorptive BrC in this study, we applied the multiple linear regression (MLR) method to attribute BrC light absorption at different wavelengths to OA components from various sources, based on the PMF analysis conducted at the YBJ and GIG sites. The detailed

393 methodology is described in Sect.2.5.

394   At the YBJ site in Tibet, the MLR model identified BBOA (the sum of BBOA and Biofuel–OA, as

395 defined in Sect.2.5.1 and Text S1), HOA, LO–OOA, and MO–OOA as the main contributors to BrC light

396 absorption. As shown in Fig. 5a, secondary organic aerosol (SOA, comprising LO–OOA and MO–OOA)

397 dominated the total OA mass concentration (67 %), followed by BBOA (22 %) and HOA (11 %).

398 However, for BrC light absorption, POA (including BBOA and HOA) emerged as the most significant

399 contributor, with BBOA contributing the most (40 %), followed by HOA (38 %) and SOA (22 %),

400 signifying the key role played by biomass burning and vehicle emissions for BrC light absorption at the

401 YBJ site. Indeed, both the BBOA (R = 0.77) and HOA (R = 0.64) show better correlations with BrC light

402 absorption at 370 nm than other factors (Fig. S10). A similar trend was observed at the GIG site in urban

403 Guangzhou (Fig. 5d), where POA (including BBOA, HOA) represented only 29 % of the total OA mass

404 concentration but contributed disproportionately to BrC light absorption (89 %). These findings highlight

405 the critical role of primary BrC in light absorption during our measurement campaign. In the following,

406 we will discuss each source contribution to BrC in detail.
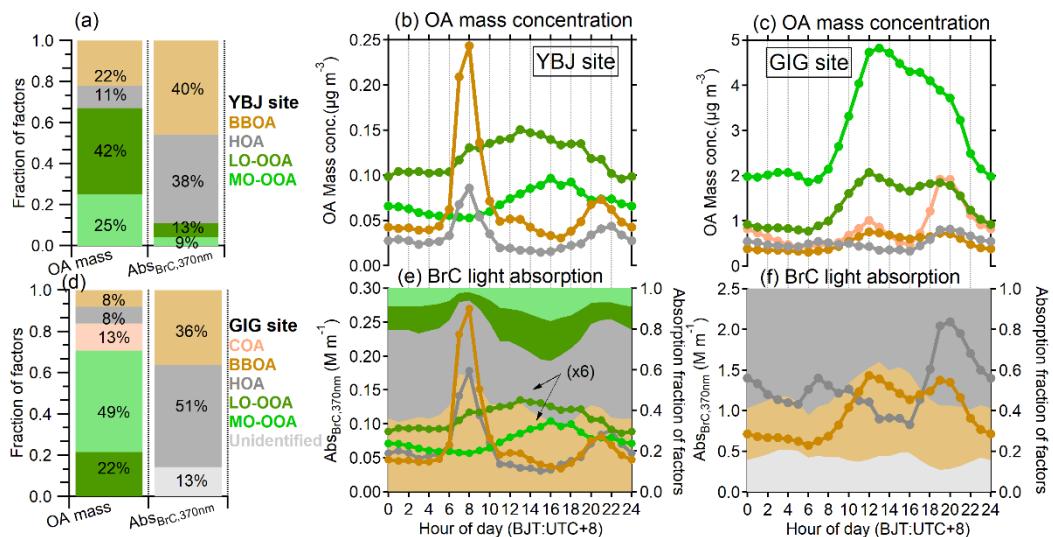
407
408 Figure 5. (a) The contributions of different OA factors to total OA (left bars) and contributions of different
409 OA factors to BrC light absorption at 370 nm (right bars) at the YBJ site and GIG site. The diurnal
410 variations of OA factors mass loading and the light absorption of different OA components at 370 nm at
411 the YBJ site (b, e) and GIG site (c, d). The "x6" indicates the light absorption of LO-OOA and MO-OOA
412 at 370 nm expanded by 6 times to better guide the eyes for the trend of diurnal patterns.

413 **3.2.1. Optical properties of BBOA**

414   The diurnal variations of the biomass burning OA (BBOA) light–absorbing coefficients at 370 nm

415 for the YBJ site exhibited strong correlation with BBOA mass concentration (Fig. 5b, 5e), characterized

416 by distinct peaks at 08:00 and 21:00 local time. This temporal pattern aligns with the observation reported

417 in urban Lhasa, which exhibits a peak at 9:00 and 22:00, respectively (Zhao et al., 2022). The BBOA

418 peaks at the YBJ site (central QTP) in the morning and night are primarily influenced by local

419 anthropogenic activities, i.e., the traditional Weisang ritual. The Weisang activity, prevalent throughout

420 Tibet, including the sparsely populated YBJ region, typically occurs twice daily in the morning and

421 evening. Wherever Tibetans are living, almost all have a Weisang furnace. This cultural practice involves

422 the combustion of specific organic materials, including wormwood, cypress branches, highland barley,

ghee lamp, and zanba in dedicated stoves, generating characteristic mulberry smoke for religious purposes (Zhang et al., 2020b; Zhang et al., 2022a). Additionally, traditional residential solid biofuel combustion (primarily yak dung and wood) for cooking and space heating contributes significantly to BBOA loading in the plumes (Shen et al., 2021). The AMS spectral similarity between ambient BBOA and emissions from both Weisang activities and solid biofuel combustion (Zhang et al., 2022a), showing the highest signals of m/z 41, 43 and 55, and high abundance of hydrocarbon ions above m/z 60, provides further evidence for their dominant contributions to regional BBOA in Tibet. The hourly wind roses show that the wind direction at the YBJ site exhibits a regular diurnal pattern, with a gradual change from the north wind in the morning to the stronger southeast wind in the afternoon (Fig. S11). Combining the Bivariate polar plots, the higher morning peak (6:00 to 11:00) of BBOA was from the nearby residential area under low wind speed condition (Figs. S12, 13), while the lower evening peak was due to the dilution of stronger wind speed in the evening (17:00 to 24:00) (Figs. S12, 13).

Compared to Tibet, the urban Guangzhou exhibited fundamentally different diurnal patterns in both BBOA mass concentration and BrC light absorption coefficients (Fig. 5c, 5f), where the BBOA peak occurs around noon and nighttime, reflecting the different biomass burning activity between Tibet and Guangzhou. Previous literature (Cai et al., 2023; Wang et al., 2017) reported that the agriculture burning at the suburban areas likely dominated the BBOA mass concentration at Guangzhou areas.

The mass absorption coefficient (MAC, $m^2\ g^{-1}$), a crucial optical parameter for BrC characterization, quantifies the light absorption capacity per unit mass of OA. Our measured MAC values for BBOA (1.11–2.54 $m^2\ g^{-1}$ at YBJ vs. 1.91 $\pm$ 0.21 $m^2\ g^{-1}$ at GIG; Table 1, S4) fall within the lower range of previously reported values (0.6–8 $m^2\ g^{-1}$; Fig. 6, Table S10). This variability in MAC values from similar combustion sources, as documented in numerous studies (Budisulistiorini et al., 2017; Chen and Bond, 2010; Martinsson et al., 2015; Saleh et al., 2014), arises from multiple factors, including fuel composition, combustion conditions, and efficiency. The relatively low MAC values observed at both sites in this study can be attributed to several reasons: 1) Both studies were conducted in the summer time, which coincided with intense solar radiation and elevated oxidant concentrations, promoting photobleaching of chromophores in fresh BBOA (Sumlin et al., 2017). Recent experimental evidence (Hems et al., 2021) demonstrates rapid (minutes to hours), nonlinear photobleaching kinetics of fresh BrC, highlighting the complex nature of these atmospheric processes. Especially for the Guangzhou samples, BBOA from regional transport was likely subjected to a longer oxidation process, which led to a lower MAC at the GIG site. 2) Combustion conditions and fuel type significantly influence MAC values (Martinsson et al., 2015). Zhang et al. (2022a) systematically characterized Tibetan biofuel emissions, revealing that Weisang materials and yak dung produce abundant OA with relatively low light absorption efficiency due to incomplete combustion. Similarly, Moschos et al. (2024) showed higher MAC values for hardwoods (0.8–1.6 $m^2\ g^{-1}$) versus animal dung (0.2–0.7 $m^2\ g^{-1}$); 3) At YBJ site, the multiple linear regression (MLR) model incorporates biofuel–OA, which contains cooking OA, typically characterized by weak/no absorption (Kasthuriarachchi et al., 2020a; Qin et al., 2018). The spectral similarity between COA and biofuel–OA prevents complete separation in PMF analyses. Sensitivity analyses (Sect.2.5.1 and Text S1; Table S5) demonstrate MAC_{BBOA} variability (1.11–2.54 $m^2\ g^{-1}$) under different model assumptions, with maximum values (2.54 $m^2\ g^{-1}$) obtained when excluding biofuel–OA contributions.

3.2.2. Optical properties of HOA

The light–absorbing coefficient of HOA at the YBJ site exhibited a pronounced peak at 08:00 and a minor peak at 22:00 (Fig. 5b, 5e), aligning with the diurnal variation of HOA mass concentration. In the Tibetan Plateau region, heavy–duty diesel trucks, which are critical for transporting essential goods across this remote area, constitute a significant emission source alongside gasoline vehicles (Liu et al., 2021; Xiang et al., 2024). Our observation site is located less than 1 km (straight-line distance) from the G6 Beijing–Tibet Expressway. The Bivariate polar plots also show that the HOA was affected by the wind direction, with the morning peak affected by the north and northeast plumes, while the evening peak was affected by the southeast and northeast plumes with stronger wind speed. The traffic emission during the night is more regional than that in the morning, which was supported by the fact that the NO mass concentration was only enhanced during the morning (2.3 ppb) but not during the night, while an obvious NO_2 peak at both periods (10 ppb and 7.2 ppb) was observed (Fig. 4a). Combining the Rose plots and Bivariate polar plots (Fig. S12), the evening peak of HOA was also affected by the southeast and northeast traffic emissions plumes with stronger wind speed, which also supported the regional nature of evening HOA peak. At the urban GIG site in Guangzhou, HOA light absorption coefficients displayed a bimodal distribution with a moderate morning peak at 07:00 and a stronger evening peak at 20:00 (Figs. 5c, 5f), consistent with typical urban traffic emissions for rush hours (Chen et al., 2021). The much higher evening peak than the morning peak coincides with rush–hour traffic congestion, suggesting intensified vehicular emissions during these periods, as well as the effects of meteorological conditions (e.g., reduced boundary layer height). The different diurnal variation of light absorption on both HOA and BBOA between Tibetan and Guangzhou observations highlights the regionally specific emission drivers from different areas.

In our study, the MAC of HOA for Tibet (2.08 ± 0.3 m^2 g^{-1}) and urban Guangzhou (2.57 ± 0.28 m^2 g^{-1}) (Table 1) were in the higher ranges of HOA MAC values reported by other studies (0.4–2.04 m^2 g^{-1}) (Table S10). Note that since the OOA factors in Guangzhou were not considered in the BrC source apportionment due to collinearity with BBOA, the HOA reported here shall be an upper limit. The results of both observation sites show that the HOA MAC (2.08 m^2 g^{-1} at YBJ site vs. 2.57 m^2 g^{-1} at GIG site) is larger than the BBOA MAC (1.11–2.54 m^2 g^{-1} at YBJ vs. 1.91 ± 0.21 m^2 g^{-1} at GIG). To investigate whether the MAC from ambient BBOA or HOA is higher, we summarized the MAC results from different field studies in Fig. 6, yet no clear conclusion can be drawn. E.g., Higher HOA MAC than BBOA was observed for central Amazon study (De Sá et al., 2019) and Mexico study (Retama et al., 2022), while much higher BBOA MAC than HOA was found for Xianghe, Athens, Paris studies (Kaskaoutis et al., 2021; Wang et al., 2019b; Zhang et al., 2020c). For emission experiments, higher MAC for diesel exhaust than crop and wood have also been observed (Cheng et al., 2011; Du et al., 2014). In addition, very strong light absorption capacity (MAC; 5–6 m^2 g^{-1}) (Table S10) induced by coal combustion (Wang et al., 2019b; Zhang et al., 2022b) was found, which is comparable to these extreme MAC values reported from biomass burning (5–7.5 m^2 g^{-1}) (Table S10) (Kaskaoutis et al., 2021; Zhang et al., 2020c). The diversity of MAC from different combustion sources implies the complex influences on light absorption from multiple factors, e.g., ambient oxidation, combustion efficiency and fuel types. The comparable and

502 diverse MAC between HOA and BBOA (Cappa et al., 2019; Zhong and Jang, 2014) warrants reevaluation

503 of traffic aerosols' climate forcing and the necessity for clarifying MAC parameterizations for different

504 sources.

505 ### 3.2.3. Optical properties of SOA

506 Compared with the diurnal variation characteristics of BBOA and HOA from local emissions at YBJ

507 site, light absorption coefficients of the less–oxidized oxygenated OA (LO–OOA) and more–oxidized

508 oxygenated factor (MO–OOA) were characterized by high values during the day and low values at night

509 (Fig. 5b, 5e). This day–enhanced temporal variation aligns with that of MO–OOA reported at NamCo

510 (an observation station in central QTP) (Xu et al., 2018), which is influenced by the enhanced secondary

511 BrC from photochemical oxidation during the day. In this study, the contribution of LO–OOA factor

512 shows a broad increase to $Abs_{BrC,370nm}$ during the day and peaks around 14:00 (20 %), while MO–OOA

513 contribution (16 %) peaks approximately two hours later (16:00). The different diurnal variation of MO–

514 OOA and LO–OOA suggests different formation pathways. In general, LO–OOA is characterized by

515 freshly formed SOA showing a higher light absorption contribution (13 %) than that of MO–OOA (9 %),

516 which more represents the regionally aging SOA (Figs. 5b, 5e). For the GIG site, the maximum direct

517 light absorption contribution from SOA incorporated into case 2 (see Sect.2.5.1 and Text S1; Tables S4

518 and S6) is 33 % (Fig. S9).

519 The MAC of SOA (LO–OOA and MO–OOA) showed much lower values (0.15 and 0.18 m² g⁻¹;

520 Table 1, Fig. 6) than primary sources (e.g., BBOA and HOA), consistent with their higher degree of

521 oxidation leading to the weaker light absorptivity of OA (Lee et al., 2014; Lambe et al., 2013). Lower

522 MAC of SOA (0–4 m² g⁻¹) (Table S10) than POA (0.4–8 m² g⁻¹) has also been observed in multiple other

523 ambient (De Sá et al., 2019; Retama et al., 2022; Tian et al., 2023; Washenfelder et al., 2015; Zhang et

524 al., 2021; Zhang et al., 2022b) and laboratory studies (Ni et al., 2021; Hems et al., 2021; Zhong and Jang,

525 2014).
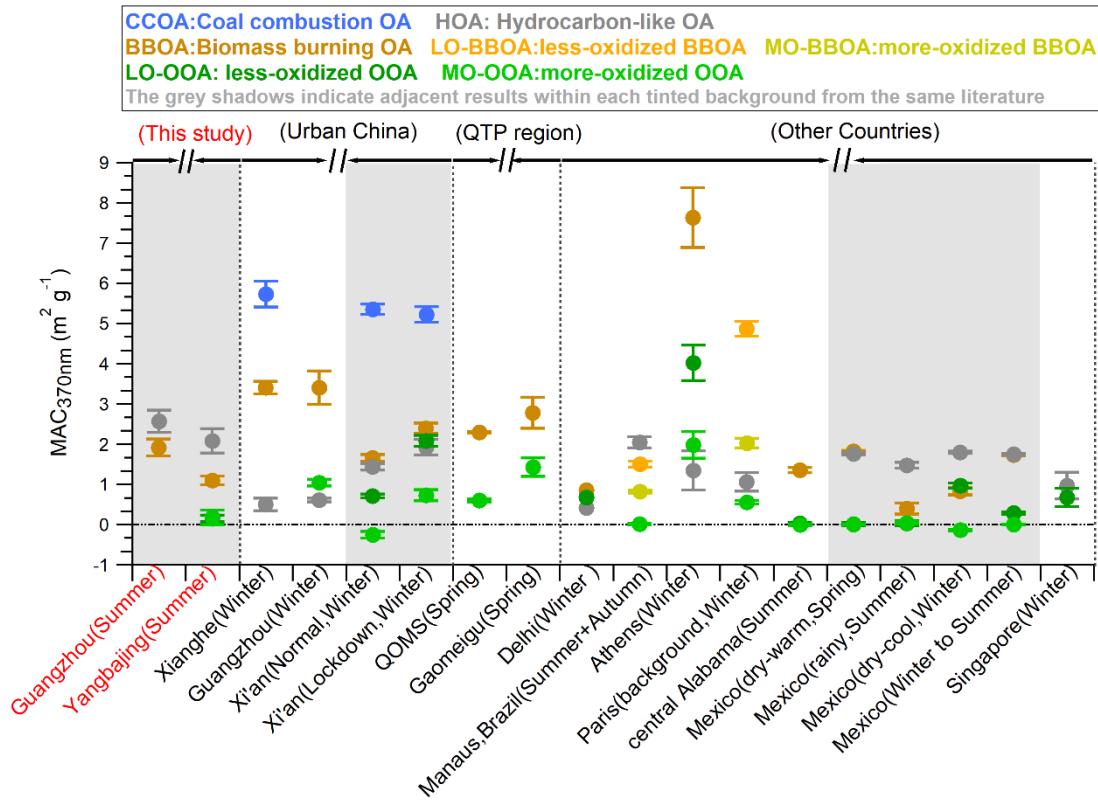
Figure 6. The literature summary of MAC from different BrC sources, which was obtained by the PMF–MLR method in different environments. All the results were categorized based on the locations of their observation sites (urban China, Qinghai–Tibet Plateau (QTP region), and other countries). Note the MO-OOA in Paris study represents OOA. Shadows indicate adjacent results within each tinted background from the same literature. The detailed information is provided in Table S10.

3.2.4. Summarized source contribution to BrC in the field studies

Figs. 7 (detailed data in Table S9) summarizes the light absorption contributions of OA from various sources across different regions, based on PMF and MLR analyses. Offline filter results are denoted by an asterisk in the pie chart. Based on this dataset, several features were found: 1) POA (primary organic aerosol) significantly influence ambient BrC light absorption on a global scale, accounting for 30–95 % of the BrC light absorption except the extremely low fraction (8.3 %) in Xi'an during summer (Lei et al., 2019). In particular, 3 quarters of the summarized study (based on number, as shown in Fig. S14) show that the POA contributes more than 50 % of BrC light absorption, signifying the important contribution of primary emission to total BrC. In the recent global model, Li et al. (2025) also found the primary emission dominated (77 %) the total light absorption from Nitrogen compounds. Note that the offline studies may underestimate the light absorption contribution of POA due to the application of soluble BrC (Bao et al., 2022; Chen et al., 2020; Lei et al., 2019; Zhong et al., 2023); 2) Key POA sources of BrC light absorption include coal combustion, biomass burning, and traffic emissions, with their light absorption contributions relative to total OA of 1–56 % (average: 33 %), 6–85 % (average: 38 %) and 4–83 % (average: 27 %), respectively (Fig. 7 and Table S9); 3) Coal combustion is especially evident in northern China during winter, with light absorption contribution of 30–89 % relative to POA (Lei et al., 2019; Sun et al., 2021; Wang et al., 2019b; Zhang et al., 2022b). In areas not subject to coal combustion, the biomass burning and traffic emissions dominate primary BrC light absorption, which can contribute

11–100 % (53 % for average) and 5–98 % (43 % for average) of primary BrC, respectively (Retama et al., 2022; De Sá et al., 2019; Kaskaoutis et al., 2021; Kasthuriarachchi et al., 2020a; Singh et al., 2021; Washenfelder et al., 2015; Zhang et al., 2020c). 4) The light absorption contribution from different sources showed significant spatial and temporal differences, e.g., HOA shows extremely high light absorption contribution in Singapore during summer (83 %), and in Mexico in both winter (54 %) and summer (49 %), while biomass burning dominated in central Alabama (85 %) and Paris (74 %). Given the pronounced spatial and temporal variations in source–specific light absorption, it is essential to conduct region–specific and season–specific observational research for a better understanding of the BrC sources and to better understand BrC sources and to better validate model simulations.
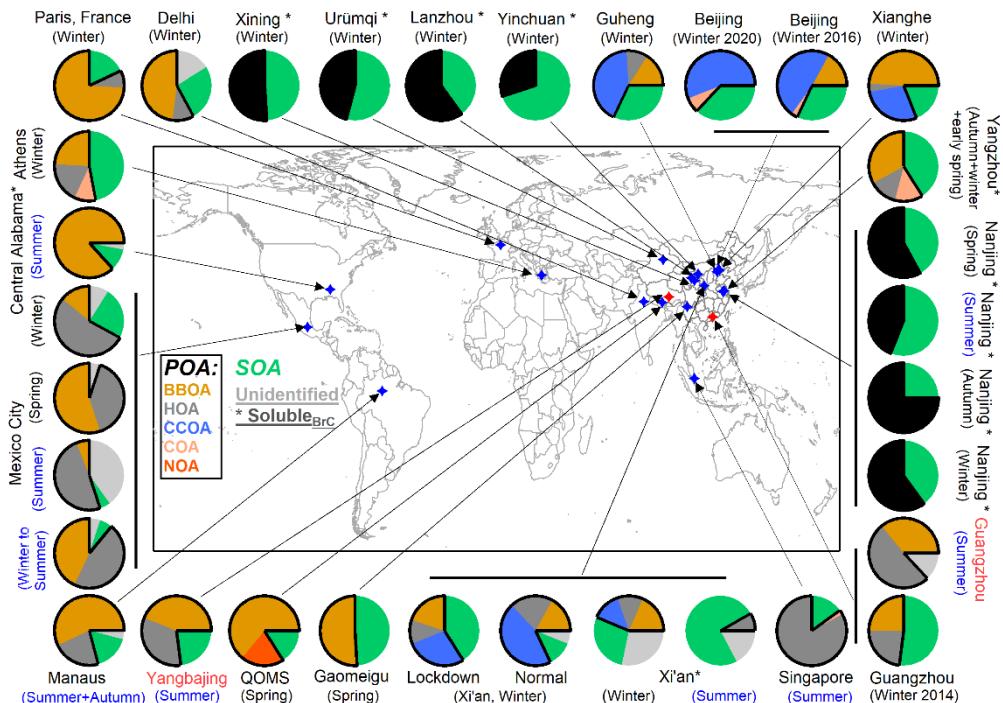
Figure 7. The summary of the contribution to BrC light absorption at 370 nm from different sources using the PMF–MLR method. The asterisks (*) represent the light absorption contributions of soluble BrC from different sources at 365nm. The sources include POA: biomass burning OA (BBOA), hydrocarbon–like OA (HOA), coal combustion OA(CCOA), cooking–related OA(COA), nitrogen-containing OA(NOA); The total SOA from oxygenated OA was used here. In addition, the unidentified fraction from the intercept of the MLR method was also shown. The detailed information on each pie is provided in Table S9.

3.3. Radiative effect of BrC from different sources

The simple forcing efficiency (SFE) of different organic aerosol (OA) components at the YBJ and GIG sites was estimated using Eq. (4) as described in Sect.2.6. This methodology has been widely applied to evaluate the climate impact of brown carbon (BrC) (Tian et al., 2023; Wang et al., 2019b; Zhang et al., 2022b; Zhong et al., 2023). As illustrated in Fig. 8, black carbon (BC) emerged as the dominant light–absorbing component, exhibiting the highest integrated SFE values of 294.7 W g^{-1} at the YBJ site and 286.3 W g^{-1} at the GIG site. In contrast, the integrated total SFE (from total OA absorption) across the 370–660 nm wavelength range was 21.4 W g^{-1} at the YBJ site and 33.8 W g^{-1} at the GIG site, representing approximately 9–13 % of the BC values. This is consistent with the well–documented strong light–absorbing properties of BC (Gustafsson and Ramanathan, 2016), while also highlighting the significant

577 role of BrC in short–term climate effects.

578   The SFE values for POA at the YBJ (19.2 W g⁻¹) and GIG (33.8 W g⁻¹) sites were comparable to

579 those observed in other urban areas, such as Xi'an (approximately 33 W g⁻¹ for HOA + BBOA + CCOA)

580 during winter (Zhang et al., 2022b). POA, including BBOA and HOA, contributed significantly to the

581 total BrC light absorption, accounting for over 80 % of the BrC-specific SFE in this study. These findings

582 underscore the substantial influence of anthropogenic emissions on aerosol radiative forcing and their

583 implications for regional and global climate systems.

584   From an environmental and climatic perspective, these results emphasize the critical role of both

585 BC and BrC in modulating atmospheric radiative balance. The higher SFE of BC underscores its potent

586 warming effect, while the non–negligible contribution of BrC, particularly from POA, highlights the

587 importance of addressing anthropogenic sources. Further elucidating the fossil and non–fossil

588 contribution, i.e., vehicle emission, coal vs. biomass burning combustion to the BrC, is vital for refining

589 climate models, informing mitigation strategies, and developing policies aimed at reducing short–lived

590 climate pollutants to mitigate near–term climate change and its associated environmental impacts.
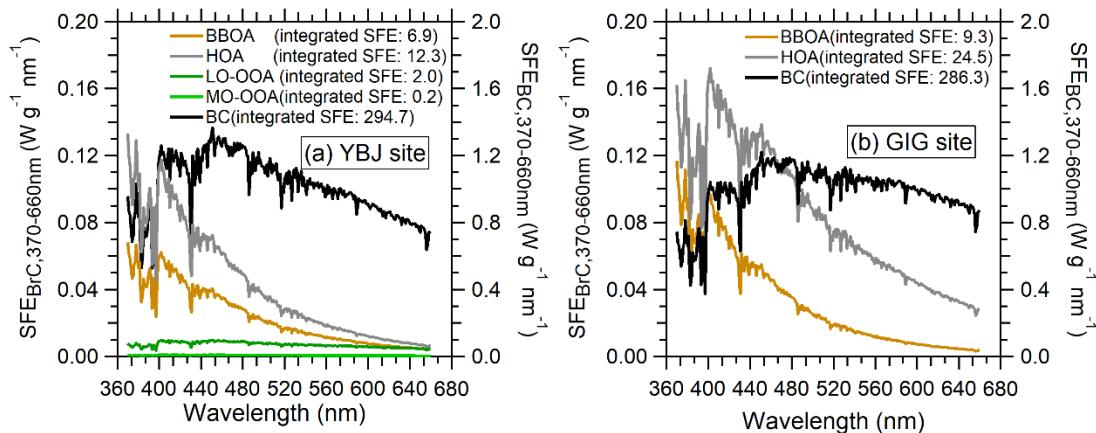
591

592 Figure 8. The Simple forcing efficiency (SFE) of BrC from different sources and BC from 370 to 660
593 nm at (a) YBJ and (b) GIG site.

594 **4.   Conclusions**

595   To explore the optical properties, source contributions, and radiative effects of BrC in Qinghai–

596 Tibet Plateau, the observations equipped with the AE33 and the SP–AMS were carried out in July 2022

597 in the Tibet background site (Yangbajing). For comparison, a simultaneous field observation was also

598 conducted at the same periods in Guangzhou, a megacity with significant anthropogenic emissions. Our

599 results reveal that the light absorption coefficient at 370nm from total aerosols (Abs_{total}, 1.6 ± 1.6 M m⁻¹)

600 and BrC (Abs_{BrC}, 0.2 ± 0.3 M m⁻¹) in Tibet were approximately an order of magnitude lower than those

601 in Guangzhou (Abs_{total}, 13.2 ± 7 M m⁻¹; Abs_{BrC}, 2.9 ± 2 M m⁻¹), consistent with the extremely low mass

602 concentrations of total aerosols and organic aerosols (OA) observed at the Tibetan site. The minimal

603 aerosol loading and weak light absorption in Tibet underscore its pristine atmospheric background.

604   Despite a large discrepancy in absolute light absorption coefficient, the BrC light absorption

605 contribution to total aerosols (15 % and 21 %) is comparable between the two sites at 370 nm,

606 highlighting BrC's significant contribution to total aerosol light absorption in Tibet. The summarized

607 field studies demonstrate a positive correlation between BrC fraction in Abs_{total} as a function of POA/OA

(R = 0.54), suggesting primary emissions contribute more effectively to BrC light absorption than BC, and POA is a more important source of BrC light absorption than SOA at these two sites. Source apportionment via the PMF–MLR method identified biomass–burning OA (BBOA) and hydrocarbon–like OA (HOA) from vehicles as the major contributors (> 80 %) to the BrC light absorption in both sites. The summarized field studies show that POA can account for 30–95 % of the BrC light absorption on a global scale. All these finding signifies the critical role of primary emission in OA light absorption. The main primary source for BrC includes biomass burning/biofuels, coal combustion, and vehicle emissions.

Diurnal variations of BrC and its sources exhibited distinct patterns with morning and nighttime peaks. Weisang activity and traffic rush hours in Tibet significantly influenced BrC levels, underscoring even remote regions' vulnerability to anthropogenic activities. Notably, traffic–related BrC contributions remain substantial in Guangzhou and even in the Tibet background, which necessitates that explicit light absorption parameters for fossil-derived BrC (e.g., from vehicle emissions) be considered in model simulations. Current literature remains inconclusive regarding MAC differences between HOA and BBOA, though fuel type, combustion efficiency, and aging effects critically influence BrC MAC, emphasizing the need for enhanced field measurements and parameterization of source-specific MACs.

Based on this field study, the integrated total SFE of BrC across the 370–660 nm wavelength range can account for approximately 7 % and 12 % of the BC (294.7 W g^{-1} in Tibet and 286.3 W g^{-1} in Guangzhou). In total, primary emission contributes over 98 % of the total SFE at both sites. These findings reinforce the urgency of controlling primary emissions and call for regional–specific parameterizations in climate models to improve assessments of BrC's radiative effects. In general, our study promotes the understanding of BrC dynamic variation and its sources at clean background Tibet and typical urban areas, emphasizing the strong influences of anthropogenic to radiative forcing.

Data availability

The data shown in the paper are available on request from the corresponding authors (weiweihu@gig.ac.cn and shanhuang_eci@jnu.edu.cn).

Author contributions

WH, SH, PY, NM, BY, MS designed the research. SH, PY, NM, BY, WZ, ZL, LL, TP, TF, JW conducted the field measurements. GZ and XB supported the AE33 instrument. WZ, LL, ZL, and YC analyzed the data. LL and SH supported the SP-AMS data analysis and OA source analysis for the Tibet campaign. WZ wrote the paper. WH, SH, ZL, TP, TF, JW, YC, GZ, XB, and XW reviewed and commented on the paper.

Competing interests.

The authors declare that they have no conflict of interest.

Acknowledgments

This work has been supported by National Natural Science Foundation of China (Grant No 42375105), the second Tibetan Plateau Scientific Expedition and Research Program (Grant No. 2019QZKK0604), International Partnership Program of Chinese Academy of Sciences (Grant No.164GJHZ2023068FN), Guangdong Foundation for Program of Science and Technology Research (Grant No 2023B1212060049), Science Fund for Creative Research Groups of the National Natural Science Foundation of China (Grant No 42321003). We appreciate Xiaomin Chen from Jinan University for providing assistance regarding PMF analysis.

References

Andreae, M. O. and Gelencsér, A.: Black carbon or brown carbon? The nature of light-absorbing carbonaceous aerosols, Atmos. Chem. Phys., 6, 3131-3148, 10.5194/acp-6-3131-2006, 2006.

Bao, M., Zhang, Y.-L., Cao, F., Lin, Y.-C., Hong, Y., Fan, M., Zhang, Y., Yang, X., and Xie, F.: Light absorption and source apportionment of water soluble humic-like substances (HULIS) in PM2.5 at Nanjing, China, Environmental Research, 206, 10.1016/j.envres.2021.112554, 2022.

Barrett, T. E. and Sheesley, R. J.: Year-round optical properties and source characterization of Arctic organic carbon aerosols on the North Slope Alaska, Journal of Geophysical Research: Atmospheres, 122, 9319-9331, 10.1002/2016jd026194, 2017.

Bond, T. C. and Bergstrom, R. W.: Light Absorption by Carbonaceous Particles: An Investigative Review, Aerosol Science and Technology, 40, 27-67, 10.1080/02786820500421521, 2006.

Bond, T. C., Bergstrom, R. W. J. A. S., and Technology: Light Absorption by Carbonaceous Particles: An Investigative Review, 40, 27 - 67, 2006.

Brown, H., Liu, X., Feng, Y., Jiang, Y., Wu, M., Lu, Z., Wu, C., Murphy, S., and Pokhrel, R.: Radiative effect and climate impacts of brown carbon with the Community Atmosphere Model (CAM5), Atmospheric Chemistry and Physics, 18, 17745-17768, 10.5194/acp-18-17745-2018, 2018.

Budisulistiorini, S. H., Riva, M., Williams, M., Chen, J., Itoh, M., Surratt, J. D., and Kuwata, M.: Light-Absorbing Brown Carbon Aerosol Constituents from Combustion of Indonesian Peat and Biomass, Environ Sci Technol, 51, 4415-4423, 10.1021/acs.est.7b00397, 2017.

Cai, Y., Ye, C., Chen, W., Hu, W., Song, W., Peng, Y., Huang, S., Qi, J., Wang, S., Wang, C., Wu, C., Wang, Z., Wang, B., Huang, X., He, L., Gligorovski, S., Yuan, B., Shao, M., and Wang, X.: The important contribution of secondary formation and biomass burning to oxidized organic nitrogen (OON) in a polluted urban area: insights from in situ measurements of a chemical ionization mass spectrometer (CIMS), Atmospheric Chemistry and Physics, 23, 8855-8877, 10.5194/acp-23-8855-2023, 2023.

Canonaco, F., Crippa, M., Slowik, J. G., Baltensperger, U., and Prévôt, A. S. H.: SoFi, an IGOR-based interface for the efficient use of the generalized multilinear engine (ME-2) for the source apportionment: ME-2 application to aerosol mass spectrometer data, Atmospheric Measurement Techniques, 6, 3649-3661, 10.5194/amt-6-3649-2013, 2013.

Cappa, C. D., Zhang, X., Russell, L. M., Collier, S., Lee, A. K. Y., Chen, C. L., Betha, R., Chen, S., Liu,

681   J., Price, D. J., Sanchez, K. J., McMeeking, G. R., Williams, L. R., Onasch, T. B., Worsnop, D. R.,

682   Abbatt, J., and Zhang, Q.: Light Absorption by Ambient Black and Brown Carbon and its

683   Dependence on Black Carbon Coating State for Two California, USA, Cities in Winter and Summer,

684   Journal of Geophysical Research: Atmospheres, 124, 1550-1577, 10.1029/2018jd029501, 2019.

685 Cappa, C. D., Onasch, T. B., Massoli, P., Worsnop, D. R., Bates, T. S., Cross, E. S., Davidovits, P., Hakala,

686   J., Hayden, K. L., Jobson, B. T., Kolesar, K. R., Lack, D. A., Lerner, B. M., Li, S.-M., Mellon, D.,

687   Nuaaman, I., Olfert, J. S., Petäjä, T., Quinn, P. K., Song, C., Subramanian, R., Williams, E. J., and

688   Zaveri, R. A.: Radiative Absorption Enhancements Due to the Mixing State of Atmospheric Black

689   Carbon, 337, 1078-1081, doi:10.1126/science.1223447, 2012.

690 Chelluboyina, G. S., Kapoor, T. S., and Chakrabarty, R. K.: Dark brown carbon from wildfires: a potent

691   snow radiative forcing agent?, npj Climate and Atmospheric Science, 7, 10.1038/s41612-024-

692   00738-7, 2024.

693 Chen, P., Kang, S., Hu, Y., Pu, T., Liu, Y., Wang, S., Rai, M., Wang, K., Tripathee, L., and Li, C.: South

694   and Southeast Asia controls black carbon characteristics of Meili Snow Mountains in southeast

695   Tibetan Plateau, Science of The Total Environment, 927, 10.1016/j.scitotenv.2024.172262, 2024.

696 Chen, W., Ye, Y., Hu, W., Zhou, H., Pan, T., Wang, Y., Song, W., Song, Q., Ye, C., Wang, C., Wang, B.,

697   Huang, S., Yuan, B., Zhu, M., Lian, X., Zhang, G., Bi, X., Jiang, F., Liu, J., Canonaco, F., Prevot,

698   A. S. H., Shao, M., and Wang, X.: Real-Time Characterization of Aerosol Compositions, Sources,

699   and Aging Processes in Guangzhou During PRIDE-GBA 2018 Campaign, Journal of Geophysical

700   Research: Atmospheres, 126, 10.1029/2021jd035114, 2021.

701 Chen, Y. and Bond, T. C.: Light absorption by organic carbon from wood combustion, Atmos. Chem.

702   Phys., 10, 1773-1787, 10.5194/acp-10-1773-2010, 2010.

703 Chen, Y., Xie, X., Shi, Z., Li, Y., Gai, X., Wang, J., Li, H., Wu, Y., Zhao, X., Chen, M., and Ge, X.: Brown

704   carbon in atmospheric fine particles in Yangzhou, China: Light absorption properties and source

705   apportionment, Atmospheric Research, 244, 10.1016/j.atmosres.2020.105028, 2020.

706 Cheng, Y., He, K. B., Zheng, M., Duan, F. K., Du, Z. Y., Ma, Y. L., Tan, J. H., Yang, F. M., Liu, J. M.,

707   Zhang, X. L., Weber, R. J., Bergin, M. H., and Russell, A. G.: Mass absorption efficiency of

708   elemental carbon and water-soluble organic carbon in Beijing, China, Atmos. Chem. Phys., 11,

709   11497-11510, 10.5194/acp-11-11497-2011, 2011.

710 Chung, C. E., Ramanathan, V., and Decremer, D.: Observationally constrained estimates of carbonaceous

711 aerosol radiative forcing, Proc Natl Acad Sci U S A, 109, 11624-11629, 10.1073/pnas.1203707109,

712 2012.

713 Chylek, P. and Wong, J.: Effect of absorbing aerosols on global radiation budget, Geophysical Research

714 Letters, 22, 929-931, https://doi.org/10.1029/95GL00800, 1995.

715 Collaud Coen, M., Weingartner, E., Apituley, A., Ceburnis, D., Fierz-Schmidhauser, R., Flentje, H.,

716 Henzing, J. S., Jennings, S. G., Moerman, M., Petzold, A., Schmid, O., and Baltensperger, U.:

717 Minimizing light absorption measurement artifacts of the Aethalometer: evaluation of five

718 correction algorithms, Atmos. Meas. Tech., 3, 457-474, 10.5194/amt-3-457-2010, 2010.

719 Corr, C. A., Hall, S. R., Ullmann, K., Anderson, B. E., Beyersdorf, A. J., Thornhill, K. L., Cubison, M.

720 J., Jimenez, J. L., Wisthaler, A., and Dibb, J. E.: Spectral absorption of biomass burning aerosol

721 determined from retrieved single scattering albedo during ARCTAS, Atmos. Chem. Phys., 12,

722 10505-10518, 10.5194/acp-12-10505-2012, 2012.

723 de Sá, S. S., Rizzo, L. V., Palm, B. B., Campuzano-Jost, P., Day, D. A., Yee, L. D., Wernis, R., Isaacman-

724 VanWertz, G., Brito, J., Carbone, S., Liu, Y. J., Sedlacek, A., Springston, S., Goldstein, A. H.,

725 Barbosa, H. M. J., Alexander, M. L., Artaxo, P., Jimenez, J. L., and Martin, S. T.: Contributions of

726 biomass-burning, urban, and biogenic emissions to the concentrations and light-absorbing

727 properties of particulate matter in central Amazonia during the dry season, Atmos. Chem. Phys., 19,

728 7973-8001, 10.5194/acp-19-7973-2019, 2019.

729 Drinovec, L., Močnik, G., Zotter, P., Prévôt, A. S. H., Ruckstuhl, C., Coz, E., Rupakheti, M., Sciare, J.,

730 Müller, T., Wiedensohler, A., and Hansen, A. D. A.: The "dual-spot" Aethalometer: an improved

731 measurement of aerosol black carbon with real-time loading compensation, Atmos. Meas. Tech., 8,

732 1965-1979, 10.5194/amt-8-1965-2015, 2015.

733 Du, Z., He, K., Cheng, Y., Duan, F., Ma, Y., Liu, J., Zhang, X., Zheng, M., and Weber, R.: A yearlong

734 study of water-soluble organic carbon in Beijing II: Light absorption properties, Atmospheric

735 Environment, 89, 235-241, 10.1016/j.atmosenv.2014.02.022, 2014.

736 Efremenko, D. and Kokhanovsky, A.: Radiative Transfer Models, in: Foundations of Atmospheric

737 Remote Sensing, edited by: Efremenko, D., and Kokhanovsky, A., Springer International Publishing,

738 Cham, 149-232, 10.1007/978-3-030-66745-0_4, 2021.

739 Feng, Y., Ramanathan, V., and Kotamarthi, V. R.: Brown carbon: a significant atmospheric absorber of

740   solar radiation?, Atmos. Chem. Phys., 13, 8607-8621, 10.5194/acp-13-8607-2013, 2013.

741 Fröhlich, R., Cubison, M. J., Slowik, J. G., Bukowiecki, N., Prévôt, A. S. H., Baltensperger, U., Schneider,

742   J., Kimmel, J. R., Gonin, M., Rohner, U., Worsnop, D. R., and Jayne, J. T.: The ToF-ACSM: a

743   portable aerosol chemical speciation monitor with TOFMS detection, Atmospheric Measurement

744   Techniques, 6, 3225-3241, 10.5194/amt-6-3225-2013, 2013.

745 Gustafsson, O. and Ramanathan, V.: Convergence on climate warming by black carbon aerosols, Proc

746   Natl Acad Sci U S A, 113, 4243-4245, 10.1073/pnas.1603570113, 2016.

747 Hems, R. F. and Abbatt, J. P. D.: Aqueous Phase Photo-oxidation of Brown Carbon Nitrophenols:

748   Reaction Kinetics, Mechanism, and Evolution of Light Absorption, ACS Earth and Space Chemistry,

749   2, 225-234, 10.1021/acsearthspacechem.7b00123, 2018.

750 Hems, R. F., Schnitzler, E. G., Liu-Kang, C., Cappa, C. D., and Abbatt, J. P. D.: Aging of Atmospheric

751   Brown Carbon Aerosol, ACS Earth and Space Chemistry, 5, 722-748,

752   10.1021/acsearthspacechem.0c00346, 2021.

753 Hu, W., Hu, M., Hu, W., Jimenez, J. L., Yuan, B., Chen, W., Wang, M., Wu, Y., Chen, C., Wang, Z., Peng,

754   J., Zeng, L., and Shao, M.: Chemical composition, sources, and aging process of submicron aerosols

755   in Beijing: Contrast between summer and winter, Journal of Geophysical Research: Atmospheres,

756   121, 1955-1977, 10.1002/2015jd024020, 2016.

757 Hu, W. W., Hu, M., Yuan, B., Jimenez, J. L., Tang, Q., Peng, J. F., Hu, W., Shao, M., Wang, M., Zeng, L.

758   M., Wu, Y. S., Gong, Z. H., Huang, X. F., and He, L. Y.: Insights on organic aerosol aging and the

759   influence of coal combustion at a regional receptor site of central eastern China, Atmospheric

760   Chemistry and Physics, 13, 10095-10112, 10.5194/acp-13-10095-2013, 2013.

761 Huang, R.-J., Yuan, W., Yang, L., Yang, H., Cao, W., Guo, J., Zhang, N., Zhu, C., Wu, Y., and Zhang, R.:

762   Concentration, optical characteristics, and emission factors of brown carbon emitted by on-road

763   vehicles, Science of The Total Environment, 810, 10.1016/j.scitotenv.2021.151307, 2022.

764 Jacobson, M. Z.: Strong radiative heating due to the mixing state of black carbon in atmospheric aerosols,

765   Nature, 409, 695-697, 10.1038/35055518, 2001.

766 Jiang, H., Frie, A. L., Lavi, A., Chen, J. Y., Zhang, H., Bahreini, R., and Lin, Y.-H.: Brown Carbon

767   Formation from Nighttime Chemistry of Unsaturated Heterocyclic Volatile Organic Compounds,

Environmental Science & Technology Letters, 6, 184-190, 10.1021/acs.estlett.9b00017, 2019.

Kang, S., Zhang, Q., Qian, Y., Ji, Z., Li, C., Cong, Z., Zhang, Y., Guo, J., Du, W., Huang, J., You, Q., Panday, A. K., Rupakheti, M., Chen, D., Gustafsson, O., Thiemens, M. H., and Qin, D.: Linking atmospheric pollution to cryospheric change in the Third Pole region: current progress and future prospects, Natl Sci Rev, 6, 796-809, 10.1093/nsr/nwz031, 2019.

Kaskaoutis, D. G., Grivas, G., Stavroulas, I., Bougiatioti, A., Liakakou, E., Dumka, U. C., Gerasopoulos, E., and Mihalopoulos, N.: Apportionment of black and brown carbon spectral absorption sources in the urban environment of Athens, Greece, during winter, Science of The Total Environment, 801, 10.1016/j.scitotenv.2021.149739, 2021.

Kasthuriarachchi, N. Y., Rivellini, L. H., Adam, M. G., and Lee, A. K. Y.: Light Absorbing Properties of Primary and Secondary Brown Carbon in a Tropical Urban Environment, Environ Sci Technol, 54, 10808-10819, 10.1021/acs.est.0c02414, 2020a.

Kasthuriarachchi, N. Y., Rivellini, L. H., Chen, X., Li, Y. J., and Lee, A. K. Y.: Effect of Relative Humidity on Secondary Brown Carbon Formation in Aqueous Droplets, Environ Sci Technol, 54, 13207-13216, 10.1021/acs.est.0c01239, 2020b.

Kirchstetter, T. W. and Thatcher, T. L.: Contribution of organic carbon to wood smoke particulate matter absorption of solar radiation, Atmos. Chem. Phys., 12, 6067-6072, 10.5194/acp-12-6067-2012, 2012.

Kirchstetter, T. W., Novakov, T., and Hobbs, P. V.: Evidence that the spectral dependence of light absorption by aerosols is affected by organic carbon, Journal of Geophysical Research: Atmospheres, 109, n/a-n/a, 10.1029/2004jd004999, 2004.

Lack, D. A. and Langridge, J. M.: On the attribution of black and brown carbon light absorption using the Ångström exponent, Atmos. Chem. Phys., 13, 10535-10543, 10.5194/acp-13-10535-2013, 2013.

Lack, D. A., Moosmuller, H., McMeeking, G. R., Chakrabarty, R. K., and Baumgardner, D.: Characterizing elemental, equivalent black, and refractory black carbon aerosol particles: a review of techniques, their limitations and uncertainties, Anal Bioanal Chem, 406, 99-122, 10.1007/s00216-013-7402-3, 2014.

Lack, D. A., Richardson, M. S., Law, D., Langridge, J. M., Cappa, C. D., McLaughlin, R. J., and Murphy, D. M.: Aircraft Instrument for Comprehensive Characterization of Aerosol Optical Properties, Part

797   2: Black and Brown Carbon Absorption and Absorption Enhancement Measured with Photo

798   Acoustic Spectroscopy, Aerosol Science and Technology, 46, 555-568,

799   10.1080/02786826.2011.645955, 2012.

800   Lambe, A. T., Cappa, C. D., Massoli, P., Onasch, T. B., Forestieri, S. D., Martin, A. T., Cummings, M. J.,

801   Croasdale, D. R., Brune, W. H., Worsnop, D. R., and Davidovits, P.: Relationship between oxidation

802   level and optical properties of secondary organic aerosol, Environ Sci Technol, 47, 6349-6357,

803   10.1021/es401043j, 2013.

804   Laskin, A., Laskin, J., and Nizkorodov, S. A.: Chemistry of atmospheric brown carbon, Chem Rev, 115,

805   4335-4382, 10.1021/cr5006167, 2015.

806   Laskin, J., Laskin, A., Nizkorodov, S. A., Roach, P., Eckert, P., Gilles, M. K., Wang, B., Lee, H. J., and

807   Hu, Q.: Molecular selectivity of brown carbon chromophores, Environ Sci Technol, 48, 12047-

808   12055, 10.1021/es503432r, 2014.

809   Lee, H. J., Aiona, P. K., Laskin, A., Laskin, J., and Nizkorodov, S. A.: Effect of Solar Radiation on the

810   Optical Properties and Molecular Composition of Laboratory Proxies of Atmospheric Brown

811   Carbon, Environmental Science & Technology, 48, 10217-10226, 10.1021/es502515r, 2014.

812   Lei, Y., Shen, Z., Zhang, T., Lu, D., Zeng, Y., Zhang, Q., Xu, H., Bei, N., Wang, X., and Cao, J.: High

813   time resolution observation of PM2.5 Brown carbon over Xi'an in northwestern China: Seasonal

814   variation and source apportionment, Chemosphere, 237, 10.1016/j.chemosphere.2019.124530,

815   2019.

816   Li, C., He, Q., Hettiyadura, A. P. S., Kafer, U., Shmul, G., Meidan, D., Zimmermann, R., Brown, S. S.,

817   George, C., Laskin, A., and Rudich, Y.: Formation of Secondary Brown Carbon in Biomass Burning

818   Aerosol Proxies through NO(3) Radical Reactions, Environ Sci Technol, 54, 1395-1405,

819   10.1021/acs.est.9b05641, 2020.

820   Li, X., Kang, S., He, X., Qu, B., Tripathee, L., Jing, Z., Paudyal, R., Li, Y., Zhang, Y., Yan, F., Li, G., and

821   Li, C.: Light-absorbing impurities accelerate glacier melt in the Central Tibetan Plateau, Sci Total

822   Environ, 587-588, 482-490, 10.1016/j.scitotenv.2017.02.169, 2017.

823   Li, Y., Fu, T.-M., Yu, J. Z., Zhang, A., Yu, X., Ye, J., Zhu, L., Shen, H., Wang, C., Yang, X., Tao, S., Chen,

824   Q., Li, Y., Li, L., Che, H., and Heald, C. L.: Nitrogen dominates global atmospheric organic aerosol

825   absorption, 387, 989-995, doi:10.1126/science.adr4473, 2025.

826   Liu, D., Whitehead, J., Alfarra, M. R., Reyes-Villegas, E., Spracklen, Dominick V., Reddington, Carly L.,

827   Kong, S., Williams, Paul I., Ting, Y.-C., Haslett, S., Taylor, Jonathan W., Flynn, Michael J., Morgan,

828   William T., McFiggans, G., Coe, H., and Allan, James D.: Black-carbon absorption enhancement in

829   the atmosphere determined by particle mixing state, Nature Geoscience, 10, 184-188,

830   10.1038/ngeo2901, 2017.

831   Liu, Y., Wang, Y., Cao, Y., Yang, X., Zhang, T., Luan, M., Lyu, D., Hansen, A. D. A., Liu, B., and Zheng,

832   M.: Impacts of COVID-19 on Black Carbon in Two Representative Regions in China: Insights

833   Based on Online Measurement in Beijing and Tibet, Geophys Res Lett, 48, e2021GL092770,

834   10.1029/2021GL092770, 2021.

835   Luo, B., Kuang, Y., Huang, S., Song, Q., Hu, W., Li, W., Peng, Y., Chen, D., Yue, D., Yuan, B., and Shao,

836   M.: Parameterizations of size distribution and refractive index of biomass burning organic aerosol

837   with black carbon content, Atmos. Chem. Phys., 22, 12401-12415, 10.5194/acp-22-12401-2022,

838   2022.

839   Martinsson, J., Eriksson, A. C., Nielsen, I. E., Malmborg, V. B., Ahlberg, E., Andersen, C., Lindgren, R.,

840   Nystrom, R., Nordin, E. Z., Brune, W. H., Svenningsson, B., Swietlicki, E., Boman, C., and Pagels,

841   J. H.: Impacts of Combustion Conditions and Photochemical Processing on the Light Absorption of

842   Biomass Combustion Aerosol, Environ Sci Technol, 49, 14663-14671, 10.1021/acs.est.5b03205,

843   2015.

844   Middlebrook, A. M., Bahreini, R., Jimenez, J. L., and Canagaratna, M. R.: Evaluation of Composition-

845   Dependent Collection Efficiencies for the Aerodyne Aerosol Mass Spectrometer using Field Data,

846   Aerosol Science and Technology, 46, 258-271, 10.1080/02786826.2011.620041, 2012.

847   Ming, J., Xiao, C., Du, Z., and Yang, X.: An overview of black carbon deposition in High Asia glaciers

848   and its impacts on radiation balance, Advances in Water Resources, 55, 80-87,

849   10.1016/j.advwatres.2012.05.015, 2013.

850   Mo, Y., Li, J., Liu, J., Zhong, G., Cheng, Z., Tian, C., Chen, Y., and Zhang, G.: The influence of solvent

851   and pH on determination of the light absorption properties of water-soluble brown carbon,

852   Atmospheric Environment, 161, 90-98, 10.1016/j.atmosenv.2017.04.037, 2017.

853   Moschos, V., Christensen, C., Mouton, M., Fiddler, M. N., Isolabella, T., Mazzei, F., Massabò, D., Turpin,

854   B. J., Bililign, S., and Surratt, J. D.: Quantifying the Light-Absorption Properties and Molecular

Composition of Brown Carbon Aerosol from Sub-Saharan African Biomass Combustion, Environmental Science & Technology, 10.1021/acs.est.3c09378, 2024.

Ni, H., Huang, R. J., Pieber, S. M., Corbin, J. C., Stefenelli, G., Pospisilova, V., Klein, F., Gysel-Beer, M., Yang, L., Baltensperger, U., Haddad, I. E., Slowik, J. G., Cao, J., Prevot, A. S. H., and Dusek, U.: Brown Carbon in Primary and Aged Coal Combustion Emission, Environ Sci Technol, 55, 5701-5710, 10.1021/acs.est.0c08084, 2021.

Onasch, T. B., Trimborn, A., Fortner, E. C., Jayne, J. T., Kok, G. L., Williams, L. R., Davidovits, P., and Worsnop, D. R.: Soot Particle Aerosol Mass Spectrometer: Development, Validation, and Initial Application, Aerosol Science and Technology, 46, 804-817, 10.1080/02786826.2012.663948, 2012.

Peng, J., Hu, M., Guo, S., Du, Z., Zheng, J., Shang, D., Levy Zamora, M., Zeng, L., Shao, M., Wu, Y. S., Zheng, J., Wang, Y., Glen, C. R., Collins, D. R., Molina, M. J., and Zhang, R.: Markedly enhanced absorption and direct radiative forcing of black carbon under polluted urban environments, Proc Natl Acad Sci U S A, 113, 4266-4271, 10.1073/pnas.1602310113, 2016.

Phillips, S. M., Bellcross, A. D., and Smith, G. D.: Light Absorption by Brown Carbon in the Southeastern United States is pH-dependent, Environ Sci Technol, 51, 6782-6790, 10.1021/acs.est.7b01116, 2017.

Powelson, M. H., Espelien, B. M., Hawkins, L. N., Galloway, M. M., and De Haan, D. O.: Brown carbon formation by aqueous-phase carbonyl compound reactions with amines and ammonium sulfate, Environ Sci Technol, 48, 985-993, 10.1021/es4038325, 2014.

Qin, Y. M., Tan, H. B., Li, Y. J., Li, Z. J., Schurman, M. I., Liu, L., Wu, C., and Chan, C. K.: Chemical characteristics of brown carbon in atmospheric particles at a suburban site near Guangzhou, China, Atmospheric Chemistry and Physics, 18, 16409-16418, 10.5194/acp-18-16409-2018, 2018.

Retama, A., Ramos-Cerón, M., Rivera-Hernández, O., Allen, G., and Velasco, E.: Aerosol optical properties and brown carbon in Mexico City, Environmental Science: Atmospheres, 2, 315-334, 10.1039/d2ea00006g, 2022.

Saleh, R.: From Measurements to Models: Toward Accurate Representation of Brown Carbon in Climate Calculations, Current Pollution Reports, 6, 90-104, 10.1007/s40726-020-00139-3, 2020.

Saleh, R., Robinson, E. S., Tkacik, D. S., Ahern, A. T., Liu, S., Aiken, A. C., Sullivan, R. C., Presto, A. A., Dubey, M. K., Yokelson, R. J., Donahue, N. M., and Robinson, A. L.: Brownness of organics in

884   aerosols from biomass burning linked to their black carbon content, Nature Geoscience, 7, 647-650,

885   10.1038/ngeo2220, 2014.

886   Shen, G., Xiong, R., Cheng, H., and Tao, S.: Rural residential energy carrier structure and primary

887   PM$_{2.5}$ emissions from the Qinghai-Tibet Plateau, Chinese Science

888   Bulletin, 66, 1900-1911, 10.1360/tb-2020-0408, 2021.

889   Singh, A., Rastogi, N., Kumar, V., Slowik, J. G., Satish, R., Lalchandani, V., Thamban, N. M., Rai, P.,

890   Bhattu, D., Vats, P., Ganguly, D., Tripathi, S. N., and Prévôt, A. S. H.: Sources and characteristics

891   of light-absorbing fine particulates over Delhi through the synergy of real-time optical and chemical

892   measurements, ATMOSPHERIC ENVIRONMENT, 252, 10.1016/j.atmosenv.2021.118338, 2021.

893   Sumlin, B. J., Pandey, A., Walker, M. J., Pattison, R. S., Williams, B. J., and Chakrabarty, R. K.:

894   Atmospheric Photooxidation Diminishes Light Absorption by Primary Brown Carbon Aerosol from

895   Biomass Burning, Environmental Science & Technology Letters, 4, 540-545,

896   10.1021/acs.estlett.7b00393, 2017.

897   Sun, J., Xie, C., Xu, W., Chen, C., Ma, N., Xu, W., Lei, L., Li, Z., He, Y., Qiu, Y., Wang, Q., Pan, X., Su,

898   H., Cheng, Y., Wu, C., Fu, P., Wang, Z., and Sun, Y.: Light absorption of black carbon and brown

899   carbon in winter in North China Plain: comparisons between urban and rural sites, Science of The

900   Total Environment, 770, 10.1016/j.scitotenv.2020.144821, 2021.

901   Tang, J., Li, J., Su, T., Han, Y., Mo, Y., Jiang, H., Cui, M., Jiang, B., Chen, Y., Tang, J., Song, J., Peng, P.

902   a., and Zhang, G.: Molecular compositions and optical properties of dissolved brown carbon in

903   biomass burning, coal combustion, and vehicle emission aerosols illuminated by excitation–

904   emission matrix spectroscopy and Fourier transform ion cyclotron resonance mass spectrometry

905   analysis, Atmospheric Chemistry and Physics, 20, 2513-2532, 10.5194/acp-20-2513-2020, 2020.

906   Tang, S., Li, F., Lv, J., Liu, L., Wu, G., Wang, Y., Yu, W., Wang, Y., and Jiang, G.: Unexpected molecular

907   diversity of brown carbon formed by Maillard-like reactions in aqueous aerosols, Chem Sci, 13,

908   8401-8411, 10.1039/d2sc02857c, 2022.

909   Tian, J., Wang, Q., Ma, Y., Wang, J., Han, Y., and Cao, J.: Impacts of biomass burning and photochemical

910   processing on the light absorption of brown carbon in the southeastern Tibetan Plateau, Atmospheric

911   Chemistry and Physics, 23, 1879-1892, 10.5194/acp-23-1879-2023, 2023.

912   Ulbrich, I. M., Canagaratna, M. R., Zhang, Q., Worsnop, D. R., and Jimenez, J. L.: Interpretation of

organic components from Positive Matrix Factorization of aerosol mass spectrometric data, Atmospheric Chemistry and Physics, 9, 2891-2918, 10.5194/acp-9-2891-2009, 2009.

Usha, K. H., Nair, V. S., and Babu, S. S.: Effects of Aerosol–Induced Snow Albedo Feedback on the Seasonal Snowmelt Over the Himalayan Region, Water Resources Research, 58, 10.1029/2021wr030140, 2022.

Wang, D., Shen, Z., Zhang, Q., Lei, Y., Zhang, T., Huang, S., Sun, J., Xu, H., and Cao, J.: Winter brown carbon over six of China's megacities: light absorption, molecular characterization, and improved source apportionment revealed by multilayer perceptron neural network, Atmospheric Chemistry and Physics, 22, 14893-14904, 10.5194/acp-22-14893-2022, 2022a.

Wang, L. Y., Qu, Y., Wang, N., Shi, J. L., Zhou, Y., Cao, Y., Yang, X. L., Shi, Y. Q., Liu, S. X., Zhu, C. S., and Cao, J. J.: Long-term spatial distribution and implication of black and brown carbon in the Tibetan Plateau, Sci Total Environ, 945, 174093, 10.1016/j.scitotenv.2024.174093, 2024.

Wang, Q., Zhou, Y., Ma, N., Zhu, Y., Zhao, X., Zhu, S., Tao, J., Hong, J., Wu, W., Cheng, Y., and Su, H.: Review of Brown Carbon Aerosols in China: Pollution Level, Optical Properties, and Emissions, Journal of Geophysical Research: Atmospheres, 127, 10.1029/2021jd035473, 2022b.

Wang, Q., Han, Y., Ye, J., Liu, S., Pongpiachan, S., Zhang, N., Han, Y., Tian, J., Wu, C., Long, X., Zhang, Q., Zhang, W., Zhao, Z., and Cao, J.: High Contribution of Secondary Brown Carbon to Aerosol Light Absorption in the Southeastern Margin of Tibetan Plateau, Geophysical Research Letters, 46, 4962-4970, 10.1029/2019gl082731, 2019a.

Wang, Q., Ye, J., Wang, Y., Zhang, T., Ran, W., Wu, Y., Tian, J., Li, L., Zhou, Y., Hang Ho, S. S., Dang, B., Zhang, Q., Zhang, R., Chen, Y., Zhu, C., and Cao, J.: Wintertime Optical Properties of Primary and Secondary Brown Carbon at a Regional Site in the North China Plain, Environmental Science & Technology, 53, 12389-12397, 10.1021/acs.est.9b03406, 2019b.

Wang, X., Heald, C. L., Liu, J., Weber, R. J., Campuzano-Jost, P., Jimenez, J. L., Schwarz, J. P., and Perring, A. E.: Exploring the observational constraints on the simulation of brown carbon, Atmospheric Chemistry and Physics, 18, 635-653, 10.5194/acp-18-635-2018, 2018.

Wang, X., Chakrabarty, R. K., Schwarz, J. P., Murphy, S. M., Levin, E. J. T., Howell, S. G., Guo, H., Campuzano-Jost, P., and Jimenez, J. L.: Dark brown carbon from biomass burning contributes to significant global-scale positive forcing, One Earth, 10.1016/j.oneear.2025.101205, 2025.

Wang, Y., Hu, M., Lin, P., Guo, Q., Wu, Z., Li, M., Zeng, L., Song, Y., Zeng, L., Wu, Y., Guo, S., Huang, X., and He, L.: Molecular Characterization of Nitrogen-Containing Organic Compounds in Humic-like Substances Emitted from Straw Residue Burning, Environmental Science & Technology, 51, 5951-5961, 10.1021/acs.est.7b00248, 2017.

Wang, Y. Q.: An Open Source Software Suite for Multi-Dimensional Meteorological Data Computation and Visualisation, Journal of Open Research Software, 7, 10.5334/jors.267, 2019.

Washenfelder, R. A., Attwood, A. R., Brock, C. A., Guo, H., Xu, L., Weber, R. J., Ng, N. L., Allen, H. M., Ayres, B. R., Baumann, K., Cohen, R. C., Draper, D. C., Duffey, K. C., Edgerton, E., Fry, J. L., Hu, W. W., Jimenez, J. L., Palm, B. B., Romer, P., Stone, E. A., Wooldridge, P. J., and Brown, S. S.: Biomass burning dominates brown carbon absorption in the rural southeastern United States, Geophysical Research Letters, 42, 653-664, https://doi.org/10.1002/2014GL062444, 2015.

Wong, J. P. S., Nenes, A., and Weber, R. J.: Changes in Light Absorptivity of Molecular Weight Separated Brown Carbon Due to Photolytic Aging, Environ Sci Technol, 51, 8414-8421, 10.1021/acs.est.7b01739, 2017.

Xiang, Y., Li, X., Zhang, T., Cheng, Q., Yan, C., Liu, X., Liu, Y., Wang, Y., Kang, S., Ding, X., and Zheng, M.: Characteristics and Sources of Organic Aerosol in PM2.5 at Yangbajing in Tibetan Plateau, Atmospheric Environment, 333, 10.1016/j.atmosenv.2024.120662, 2024.

Xie, M., Hays, M. D., and Holder, A. L.: Light-absorbing organic carbon from prescribed and laboratory biomass burning and gasoline vehicle emissions, Sci Rep, 7, 7318, 10.1038/s41598-017-06981-8, 2017.

Xu, J., Zhang, Q., Shi, J., Ge, X., Xie, C., Wang, J., Kang, S., Zhang, R., and Wang, Y.: Chemical characteristics of submicron particles at the central Tibetan Plateau: insights from aerosol mass spectrometry, Atmospheric Chemistry and Physics, 18, 427-443, 10.5194/acp-18-427-2018, 2018.

Xu, L., Lin, G., Liu, X., Wu, C., Wu, Y., and Lou, S.: Constraining Light Absorption of Brown Carbon in China and Implications for Aerosol Direct Radiative Effect, Geophysical Research Letters, 51, 10.1029/2024gl109861, 2024.

Yao, T., Thompson, L. G., Mosbrugger, V., Zhang, F., Ma, Y., Luo, T., Xu, B., Yang, X., Joswiak, D. R., Wang, W., Joswiak, M. E., Devkota, L. P., Tayal, S., Jilani, R., and Fayziev, R.: Third Pole Environment (TPE), Environmental Development, 3, 52-64, 10.1016/j.envdev.2012.04.002, 2012.

971 Yu, L., Smith, J., Laskin, A., George, K. M., Anastasio, C., Laskin, J., Dillner, A. M., and Zhang, Q.:

972   Molecular transformations of phenolic SOA during photochemical aging in the aqueous phase:

973   competition among oligomerization, functionalization, and fragmentation, Atmospheric Chemistry

974   and Physics, 16, 4511-4527, 10.5194/acp-16-4511-2016, 2016.

975 Yue, S., Bikkina, S., Gao, M., Barrie, L. A., Kawamura, K., and Fu, P.: Sources and Radiative Absorption

976   of Water-Soluble Brown Carbon in the High Arctic Atmosphere, Geophysical Research Letters, 46,

977   14881-14891, 10.1029/2019gl085318, 2019.

978 Yue, S., Zhu, J., Chen, S., Xie, Q., Li, W., Li, L., Ren, H., Su, S., Li, P., Ma, H., Fan, Y., Cheng, B., Wu,

979   L., Deng, J., Hu, W., Ren, L., Wei, L., Zhao, W., Tian, Y., Pan, X., Sun, Y., Wang, Z., Wu, F., Liu,

980   C.-Q., Su, H., Penner, J. E., Pöschl, U., Andreae, M. O., Cheng, Y., and Fu, P.: Brown carbon from

981   biomass burning imposes strong circum-Arctic warming, One Earth, 5, 293-304,

982   10.1016/j.oneear.2022.02.006, 2022.

983 Zhai, J., Yang, X., Li, L., Bai, B., Liu, P., Huang, Y., Fu, T.-M., Zhu, L., Zeng, Z., Tao, S., Lu, X., Ye, X.,

984   Wang, X., Wang, L., and Chen, J.: Absorption Enhancement of Black Carbon Aerosols Constrained

985   by Mixing-State Heterogeneity, Environmental Science & Technology, 56, 1586-1593,

986   10.1021/acs.est.1c06180, 2022.

987 Zhang, Q., Jimenez, J. L., Canagaratna, M. R., Ulbrich, I. M., Ng, N. L., Worsnop, D. R., and Sun, Y.:

988   Understanding atmospheric organic aerosols via factor analysis of aerosol mass spectrometry: a

989   review, Anal Bioanal Chem, 401, 3045-3067, 10.1007/s00216-011-5355-y, 2011.

990 Zhang, Q., Shen, Z., Zhang, L., Zeng, Y., Ning, Z., Zhang, T., Lei, Y., Wang, Q., Li, G., Sun, J., Westerdahl,

991   D., Xu, H., and Cao, J.: Investigation of Primary and Secondary Particulate Brown Carbon in Two

992   Chinese Cities of Xi'an and Hong Kong in Wintertime, Environmental Science & Technology, 54,

993   3803-3813, 10.1021/acs.est.9b05332, 2020a.

994 Zhang, X., Xu, J., and Kang, S.: Chemical characterization of submicron particulate matter (PM1)

995   emitted by burning highland barley in the northeastern part of the Qinghai–Tibet Plateau,

996   Atmospheric Environment, 224, 10.1016/j.atmosenv.2020.117351, 2020b.

997 Zhang, X., Xu, J., Zhai, L., and Zhao, W.: Characterization of Aerosol Properties from the Burning

998   Emissions of Typical Residential Fuels on the Tibetan Plateau, Environ Sci Technol,

999   10.1021/acs.est.2c04211, 2022a.

Zhang, X., Xu, J., Kang, S., Sun, J., Shi, J., Gong, C., Sun, X., Du, H., Ge, X., and Zhang, Q.: Regional Differences in the Light Absorption Properties of Fine Particulate Matter Over the Tibetan Plateau: Insights From HR-ToF-AMS and Aethalometer Measurements, Journal of Geophysical Research: Atmospheres, 126, 10.1029/2021jd035562, 2021.

Zhang, Y., Wang, Q., Tian, J., Li, Y., Liu, H., Ran, W., Han, Y., Prévôt, A. S. H., and Cao, J.: Impact of COVID-19 lockdown on the optical properties and radiative effects of urban brown carbon aerosol, Geoscience Frontiers, 13, 101320, https://doi.org/10.1016/j.gsf.2021.101320, 2022b.

Zhang, Y., Albinet, A., Petit, J.-E., Jacob, V., Chevrier, F., Gille, G., Pontet, S., Chrétien, E., Dominik-Ségue, M., Levigoureux, G., Močnik, G., Gros, V., Jaffrezo, J.-L., and Favez, O.: Substantial brown carbon emissions from wintertime residential wood burning over France, Science of The Total Environment, 743, 10.1016/j.scitotenv.2020.140752, 2020c.

Zhao, R., Lee, A. K. Y., Huang, L., Li, X., Yang, F., and Abbatt, J. P. D.: Photochemical processing of aqueous atmospheric brown carbon, Atmospheric Chemistry and Physics, 15, 6087-6100, 10.5194/acp-15-6087-2015, 2015.

Zhao, W., Zhang, X., Zhai, L., Shen, X., and Xu, J.: Chemical characterization and sources of submicron aerosols in Lhasa on the Qinghai–Tibet Plateau: Insights from high-resolution mass spectrometry, Science of The Total Environment, 152866, 10.1016/j.scitotenv.2021.152866, 2022.

Zhao, Z., Cao, J., Shen, Z., Xu, B., Zhu, C., Chen, L.-W. A., Su, X., Liu, S., Han, Y., Wang, G., and Ho, K.: Aerosol particles at a high-altitude site on the Southeast Tibetan Plateau, China: Implications for pollution transport from South Asia, 118, 11,360-311,375, https://doi.org/10.1002/jgrd.50599, 2013.

Zhong, M. and Jang, M.: Dynamic light absorption of biomass-burning organic carbon photochemically aged under natural sunlight, Atmos. Chem. Phys., 14, 1517-1525, 10.5194/acp-14-1517-2014, 2014.

Zhong, M., Xu, J., Wang, H., Gao, L., Zhu, H., Zhai, L., Zhang, X., and Zhao, W.: Characterizing water-soluble brown carbon in fine particles in four typical cities in northwestern China during wintertime: integrating optical properties with chemical processes, Atmos. Chem. Phys., 23, 12609-12630, 10.5194/acp-23-12609-2023, 2023.

Zhu, C.-S., Qu, Y., Huang, H., Shi, J.-L., Dai, W.-T., Zhang, N.-N., Wang, N., Wang, L.-Y., Ji, S.-S., and Cao, J.-J.: Brown Carbon From Biomass Burning Reinforces the Himalayas and Tibetan Plateau Warming, Geophysical Research Letters, 51, e2023GL107269,

1029 https://doi.org/10.1029/2023GL107269, 2024.

1030 Zhu, C.-S., Cao, J.-J., Hu, T.-F., Shen, Z.-X., Tie, X.-X., Huang, H., Wang, Q.-Y., Huang, R.-J., Zhao, Z.-

1031 Z., Močnik, G., and Hansen, A. D. A.: Spectral dependence of aerosol light absorption at an urban

1032 and a remote site over the Tibetan Plateau, Science of The Total Environment, 590-591, 14-21,

1033 https://doi.org/10.1016/j.scitotenv.2017.03.057, 2017.

1034 Zhu, C. S., Qu, Y., Huang, H., Chen, J., Dai, W. T., Huang, R. J., and Cao, J. J.: Black Carbon and

1035 Secondary Brown Carbon, the Dominant Light Absorption and Direct Radiative Forcing

1036 Contributors of the Atmospheric Aerosols Over the Tibetan Plateau, Geophysical Research Letters,

1037 48, 10.1029/2021gl092524, 2021.

1038